SIRTEM: Spatially Informed Rapid Testing for Epidemic Modeling and Response to COVID-19*

JAEJIN LEE, FAHIM TASNEEMA AZAD, GIULIA PEDRIELLI, and K. SELÇUK CANDAN, School of Computing, Informatics, and Decision Systems Eng., Arizona State University, USA

GERARDO CHOWELL-PUENTE, Dept. of Population Health Sciences, Georgia State University, USA

COVID-19 outbreak was declared a pandemic by the World Health Organization (WHO) on March 11, 2020. To minimize casualties and the impact on the economy, various mitigation measures have being employed with the purpose to slow the spread of the infection, such as complete lockdown, social distancing, and random testing. The key contribution of this paper is twofolds. Firstly, we present a novel extended spatially-informed epidemic model, *SIRTEM, Spatially Informed Rapid Testing for Epidemic Modeling and Response to Covid-19*, that integrates a multi-modal testing strategy considering test accuracies. Our second contribution is an optimization model to provide a cost-effective testing strategy when multiple test types are available. The developed optimization model incorporates realistic spatially based constraints, such as testing capacity and hospital bed limitation as well.

Additional Key Words and Phrases: COVID-19, multi-accuracy testing, multi-city mixing

ACM Reference Format:

Jaejin Lee, Fahim Tasneema Azad, Giulia Pedrielli, K. Selçuk Candan, and Gerardo Chowell-Puente. 2021. SIRTEM: Spatially Informed Rapid Testing for Epidemic Modeling and Response to COVID-19. 1, 1 (November 2021), 36 pages. https://doi.org/10.1145/nnnnnnn.nnnnnnn

1 INTRODUCTION

On December 31, 2019, the first COVID-19 outbreak was reported in Wuhan, China. Since then, the infection has spread rapidly and a worldwide pandemic was declared by the World Health Organization (WHO) on March 11, 2020. As of April 19, 2021, about 141.057 million cases and 3.015 million deaths have been reported [78]. Although tragic, the loss of human life is not the only cost of this pandemic. Economists forecast that the world economy will plunge about 2.4%∼3% in GDP (86.6 trillion dollars) [70]. To minimize casualties and the impact on the economy, various mitigation measures are being employed with the purpose to slow the spread of the infection, such as complete lockdown, social distancing, and random testing. Governments worldwide have chosen to employ these mitigation methods in different combinations and levels depending on their cultural background, political systems, and social consensus [4]. Screening

*This research is supported by NSF#2026860 "RTEM: Rapid Testing as Multi-fidelity Data Collection for Epidemic Modeling", NSF#1610282 "DataStorm: A Data Enabled System for End-to-End Disaster Planning and Response", NSF#1633381 "BIGDATA: Discovering Context-Sensitive Impact in Complex Systems", and NSF#1909555 "pCAR: Discovering and Leveraging Plausibly Causal (p-causal) Relationships to Understand Complex Dynamic Systems". Results were obtained using the Chameleon testbed supported by the NSF.

Authors' addresses: Jaejin Lee, jlee105@asu.edu; Fahim Tasneema Azad, fazad@asu.edu; Giulia Pedrielli, Giulia.Pedrielli@asu.edu; K. Selçuk Candan, candan@asu.edu, School of Computing, Informatics, and Decision Systems Eng., Arizona State University, USA; Gerardo Chowell-Puente, gchowell@gsu.edu, Dept. of Population Health Sciences, Georgia State University, USA.

Manuscript submitted to ACM

of the infected individuals from the uninfected susceptible population through isolation and quarantine is often enabled by diagnostic testing. Empirical data has shown this to be an effective form of prevention [76].

Any effective action plan for stopping the spread of a virus requires quantitative understanding of the dynamical evolution of the disease, and of the impact of policy measures on such dynamics. In fact, it is key to develop effective models that enable the analysis of the rate of transmission of the disease, the spread at different spatial scales, and the assessment of the effect of travel restrictions, school closures, therapeutics to manage the disease. Such models require foundational epidemiological understanding and, importantly, a possibly large volume of diverse data. In particular, testing can be seen as an important, and controllable, source of data at different fidelities. Diagnostic tests can be developed with different costs and accuracy (sensitivity and specificity). Testing is fundamental to identify outbreaks, and, if performed at *reasonable* scale, it can provide a snapshot of the evolution of the epidemic. Testing becomes even more crucial in presence of a disease that has important asymptomatic spread and is highly infectious. This was the case for Sars-CoV2. Summarizing, testing strategies should be designed with three, core, objectives:

- Objective 1: Obtain a faithful picture of the COVID-19 model as well as epidemic trajectory;
- Objective 2: Identify individuals and populations who are at risk of exposure or are already sick;
- Objective 3: Guide intervention efforts, such as isolation of infectious individuals, quarantine of the suspected contacts, and minimization of the contact rates without completely disrupting the society.

Nonetheless, testing is expensive, difficult, and creating a timely and accurate test against a new and growing epidemic is not always feasible. CDC, for example, reportedly shunned the World Health Organization (WHO) test guidelines for COVID-19 and set out to create a more advanced test. But the test failed in the field as it correctly identified COVID-19, but it falsely flagged other harmless viruses in the samples [54]. The testing program in Italy also created controversy: experts at the WHO and the Italian Health Ministry argued that Lombardy had created an inflated perception of the threat by including in case totals people who tested positive for the virus but who had not gotten sick. Other experts argue that tracking even mild cases of the virus is essential to containing its spread [82]. Research indicates that an individual infected with COVID-19 in the absence of symptoms could spread the virus to a susceptible population [82]. This potentially necessitates us to test individuals randomly to discriminate infected individuals without symptoms in addition to the testing for the individuals showing COVID-19 like symptoms. “Surveillance testing” of hundreds of people in possible hotspots helped epidemiologists in several countries tracking the spread of the epidemics before large numbers of people turn up at hospitals [71]

Yet, the decision on the daily testing rate of random tests and the symptomatic test is an essential issue for policymakers to balance virus spreading and testing costs. When policymakers implement a particular testing strategy, they need to consider multi-faceted aspects and practical limitations in employing a particular testing policy. In fact, different data collection and testing modalities and strategies available to help generating models and predicting spread/severity of a disease, have varying costs, response times, and accuracies. For instance, accuracy of available tests can have significant impact on the epidemic progress: When test sensitivity accuracy is low, we will not be able to separate the infected population efficiently from the healthy population, resulting in a spike in disease spread. On the other hand, if the specificity accuracy is low, we falsely quarantine healthy individuals. Consequently, widespread testing of asymptomatic people has the potential of disrupting the economy and affect the care infrastructures in the presence of tests with high rates of false positives. On the other hand, the testing strategy should account for several practical constraints, such as the daily testing capacity, limitations for different testing types and the potential of the epidemic to disrupt the healthcare infrastructure if we fail in identifying dangerous outbreaks. For this, we need to account for

1) the spatial distribution and mobility of the susceptible population, 2) the sensitivity and specificity of the tests, 3) how quickly results are obtained, 4) the maximum number of tests administered per day, and others. Given the above challenges, several critical questions arise:

- "What is the value of testing?"
- "Should we only test sick people for virus detection?"
- "How should we handle limited testing capacity?"
- "How much resources should be devoted to the development of highly accurate tests (low false positives, low false negatives)?"
- " Should we only use one type of test aiming at the best cost/effectiveness trade off or should we rather adopt a non-homogeneous testing policy?"
- "How do we account for spatial distribution of the populations and their movements in developing testing strategies?"

Motivated by the aforementioned questions, in this paper, we develop a spatially informed model, SIRTEM, which couples the spatio-temporal dynamics of the COVID-19 epidemic with multiple testing modalities to solve the optimal cost-effective multi-modal Covid-19 testing strategy problem while satisfying practical constraints.

Organization of the Paper. The remainder of the paper is organized as follows. We review the relevant literature in section 2. Section 3 presents the overall approach with relevant models and optimizers. Sections 3.1.1-3.1.2 present the single city and multiple city epidemiological models, respectively, while Section 3.2 presents the optimization model. Section 4 presents the numerical analysis and Section 5 draws the conclusions.

2 RELEVANT LITERATURE

Epidemic studies generally focus on (a) predicting the progress of an epidemiological phenomenon over time (Section 2.1); (b) analyzing the effects of mitigation policies over the spread of the disease; and (c) evaluating the effectiveness of diagnostic testing in reducing the spread of the disease in early stages or when no vaccines are available [74]. In this section, we will briefly review the related literature within these three areas with particular focus on COVID-19.

2.1 Epidemiological Modeling

After Bernoulli devised the first mathematical epidemiology model to estimate the mortality rate due to smallpox in 1766, a plethora of epidemiological models have been proposed with increasing presence of data driven techniques in place of or embedded with the more traditional differential equations typically used to describe the evolution of a disease across time and space. The review presented in Wei et al. [20] classifies epidemiological models into three categories: (i) Mathematical Model, (ii) Complex network model, (iii) Agent based model.

Analytical Evolutionary Models. These models are implemented as systems of differential equations and can be deterministic or stochastic [20, 28]. The most commonly used deterministic models to date are the SEIR, SIR, and SIS approaches and their extensions [1–3, 21, 35, 36, 43, 47, 52**?**]. COVID-19 has also been studied through this lens. As an example, quarantine and hospitalization augmented SEIR model have been proposed to investigate the dynamics of the Covid-19 outbreak in Hubei (China) [33], while a fractional order SEIR model was proposed for analyzing the spread within the US [80]. For the class of *stochastic models*, an common example is the Reed-Frost method [5, 9], which uses a binomial process to describe the transmission of the virus between two individuals. Such approach has been proposed to extend the SEIR model in [45], focusing on the spread of Cholera. A similar approach was used in [42] to study the Ebola

outbreak in Congo (1995). More recently, several SEIR variants were proposed to investigate the progress of COVID-19 and the effectiveness of mitigation strategies [6, 7, 13, 23, 24, 32, 46, 51, 57, 81].

Network-based Models. This class of models is traditionally adopted to understand the effect of person-to-person interaction dynamics over the spread of the disease. According to this approach, the evolution of the disease is encoded as a space-time graph, where the nodes represent individuals, and edges the interactions [20]. Due to the level of detail, network models typically are not used for large scale studies due to the computational complexity.

Agent-based Models. Similar to the case of networked models, agent-based approaches focus on individual to individual interaction and behavior (e.g., mobility, choice). This allows to analyze transmission of the virus in high resolution and embedding the effect of individual level actions on the epidemic development. Several epidemic models of this type have been investigated for Dengue, Syphilis, AIDS and Ebola [12, 16, 26, 29, 31, 49, 64, 68]. In the scope of the COVID-19 pandemic, various studies have been conducted with agent-based modeling [18, 34, 37, 38, 62, 65, 69, 73, 79]. However, also in this case, only small case studies cane be conducted due to the high computational demand.

2.2 Effects of Mitigation Policies

In the early phases of a new disease, mitigation strategies are the key to attempt controlling the increase of cases [66]. Strategies normally considered include individual recommendations, community and state-level mandates such as lockdown, social distancing, and mass testing. Different combinations of such policies have been implemented amid the COVID-19, thus motivating research in the understanding of the efficacy of such measures in reducing the spread of the disease [40, 59, 63]. In this regard, Chu et al. [15] investigated the effect that measures such as mask wearing, eyes protection, and social distancing had on the reduction in cases. As part of the analysis, the authors estimated the effect of wearing face masks, eye protection, and distancing over 1[m], was a reduction of 14.3%, 10.6%, and 10.4% in number of infections, respectively. Eikenberry et al. [22] incorporated the effect of wearing a face mask in the SEIR-based epidemic model, by modulating the time-varying infection rate within the SEIR model. Similarly, Ngonghala et al. [53] embedded the effect of the face mask in the SEIR-based model, not only using a time varying infection rate, but also using control variable to represent the the level of mask wearing thus impacting the contact rate of the SEIR model. Milne et al. [50] devised an agent based model to simulate person to person virus transmission, thus allowing the detailed analysis of small scale effects of social distancing. However. as previously mentioned, such approach cannot be used in the context of large scale analysis. Kim et al. [39] investigated the effect of school closure in South Korea using a SEIR model with population stratified by age. In this study, the authors use the confirmed cases as a proxy for the number of infected individuals in the model. However, confirmed cases are a result of testing of a minimal percentage of the population, while the actual count of the infected population is censored. Greenstone and Nigam [30] investigated the nationwide social distancing effect on the mortality rate. The authors estimate the value of social distancing to $8 trillion as the value the American population is willing to pay to decrease of COVID-19 casualties.

2.3 Effects of Diagnostic Testing

Individuating the infected individuals from the susceptible population is crucial to slow disease spread. Social distancing, as well as lockdown measures are among the most effective, and also expensive (economically as well as socially), ways to perform such separation. Testing can represent a less socially expensive alternative by allowing to target populations that require isolation [44, 55, 67]. In fact, the effect of testing during the pandemic has become the focus of several contributions. As an example, Toshikazu et al. [41] investigated the efficacy of mass testing and social distancing. The authors analysis reveals that 80% of diagnostic testing on the population combined with 30% reduction in contact

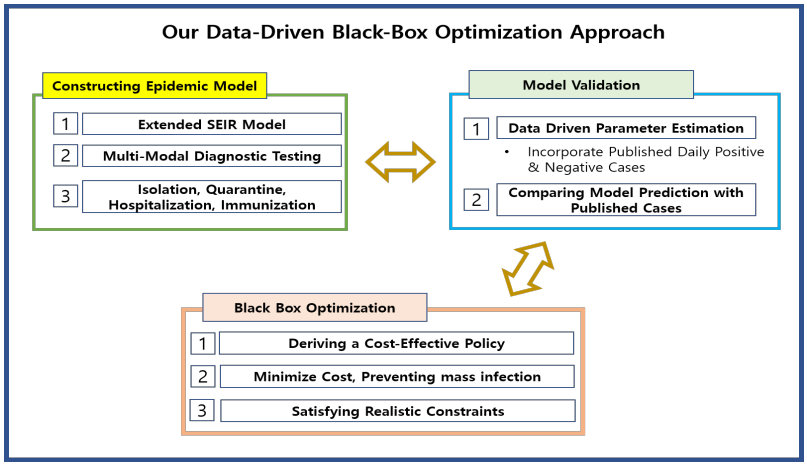

Fig. 1. Our approach: spatially-informed, coupled epidemic/testing modelling and black-box optimization

rates (attainable by implementing social distancing) could halt the pandemic in Japan. The authors do not differentiate symptomatic from randomized testing, and the work focuses on understanding the ideal extent of testing efforts. Facundo et al. [60] studied the efficacy of quarantine and testing in terms of overall resulting economical cost. Unlike the previous contribution, the authors consider symptomatic and randomized tests for a single testing method. Also, they incorporate hospitalization and immunization into the simulation model. However, they do not consider the test accuracy. However, test accuracy rose as a key aspect in evaluating effectiveness of testing based policies and analyses [19]. Incorrect diagnoses will increase economical costs (false positives), or incidence of the disease (false negatives). David et al. [56] proposed a cost-effective screening strategy for a 5,000 student college campus. They showed that testing every two days with sensitivity less than 70% could keep the infected population under control. However, extending such testing rates to a larger population could be not realistic primarily due to the lack of analysis capabilities for accurate test whose results are produced by labs with finite capacity. Similarly, Panovska et al. [58] provided the optimal testing strategy and analysis to reopen schools in the U.K. The authors proposed a stochastic model that simulates the disease transmission among individuals. In addition, Wells et al. [77] investigated the possibility of reducing the quarantine period using different testing strategies. The authors suggested that shortened quarantine period with exit testing could be an effective alternative for 14 days full quarantine.

2.4 Contributions

In this paper, we extend the SEIR model into SIRTEM "Spatially Informed Rapid Testing for Epidemic Modeling and Response to Covid-19" , an epidemic spread compartment model that takes into account isolation, quarantine, and hospitalization processes, and, most prominently, multiple tests are considered with varying accuracy and costs. In particular, we consider the test sensitivity (i.e., ability to identify positive cases - error of Type 1), and specificity (ability to identify correctly negative cases - error of Type 2).

The SIRTEM model builds on the SEIR model, but is significantly extended to reflect testing, quarantine, and hospitalizations. The model is designed to apply different testing rates for the symptomatic and asymptomatic individuals; for instance, a higher testing rate for the symptomatic individuals could be a more effective testing strategy than

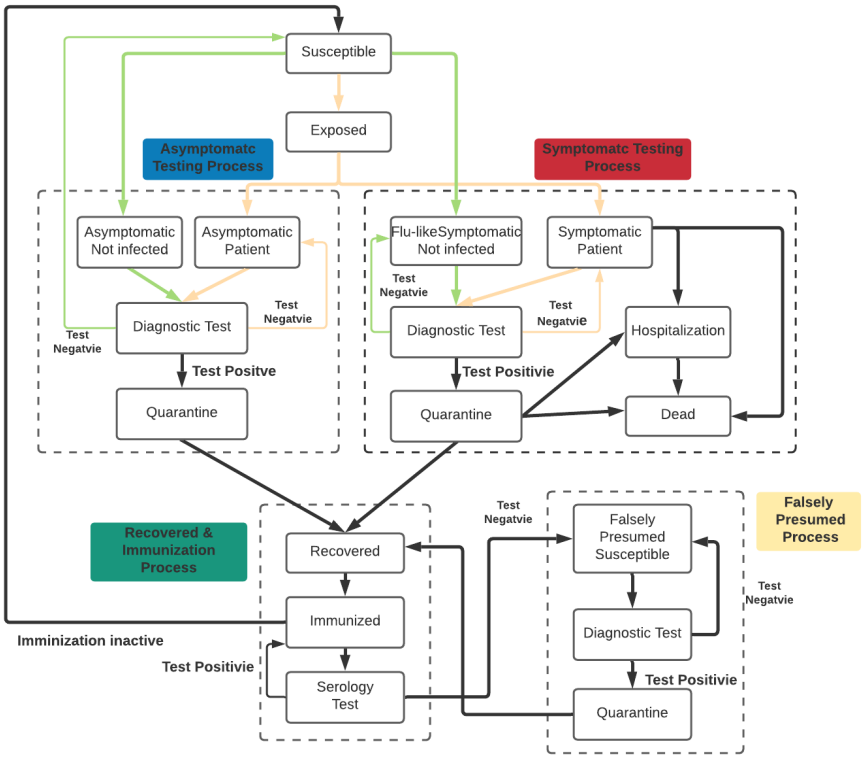

Fig. 2. Overview of the SIRTEM coupled epidemic/testing model (components, sub-components, and transitions) – for simplicity, the figure ignores the spatial scope of the underlying process

applying the same testing rate to both individuals. SIRTEM is spatially-informed since it takes into account the spatial distribution of populations as well as their non-homogeneous mixing patterns.

SIRTEM model allows the positive and negative confirmed cases to help predict the disease's propagation. Based on the SIRTEM model, we develop a nonlinear black-box optimization approach to help identify the best possible testing strategy, taking account daily testing capacities and hospitals physical bed limitations, testing, hospitalization, and quarantine costs. We separate asymptomatic and symptomatic testing, and consider multiple testing options with different levels of cost and accuracy.

3 PROPOSED APPROACH

In this paper, we take a three-step approach to testing policy development (Figure 1): (i) we develop a *spatially-informed and coupled* SIRTEM model that includes multi-modal diagnostic testing policies combined with isolation, quarantine, hospitalization, and immunization; (ii) we propose a custom estimation algorithm to calibrate the simulation parameters of the model – this approach exploits available information on hospitalizations, deaths, positive and negative cases daily; and (iii) we formulate and solve the problem of optimal testing considering the economical cost of quarantine, hospitalization, death, and testing, under constrained resources (e.g., hospital bed, testing).

Table 1. SIRTEM model parameters

Parameters	Description
tp_i	Sensitivity of diagnostic test i
tn_i	Specificity of diagnostic test i
τ_i	Time to obtain the result for diag. test i (days)
ϕ_i	Testing rate for diagnostic test i the symptomatic population (ratio per day)
ϕ_{ai}	Testing rate for diagnostic test i the non-symptomatic population (ratio per day)
tp_{se}	Sensitivity of the serology test
tn_{se}	Specificity of the serology test
τ_{se}	Time to obtain the result for the serology test (days)
ϕ_{se}	Testing rate for the serology test (ratio of the relevant population per day)
β	Infection rate for the susceptible population (ratio) = transmission rate × contact rate for the susceptible population
β'	Infection rate for the population of individuals who are falsely presumed immune (ratio) = transmission rate × contact rate for the presumed immune population
r	The ratio of the transmission rate of asymptomatic individuals to the transmission rate of symptomatic individuals
per_a	Percentage of individuals with COVID-19 who are asymptomatic
per_s	Percentage of individuals with COVID-19 who are symptomatic
η	Incubation length (days)
λ_a	Length of recovery for asymptomatic individuals (days)
λ_s	Length of recovery for symptomatic individuals (days)
λ_q	Length of quarantine (days)
λ_h	Hospitalization length (days)
h	Hospitalization rate (ratio of the quarantined population, per day)
κ	Mortality rate for symptomatic population (per day)
κ_h	Mortality rate for the hospitalized individuals (per day)
g	Ratio of the susceptible individuals who has fever and cough for non-COVID infections (ratio, per day)

3.1 SIRTEM Models

We first introduce the model for single city (Section 3.1.1) and then extend the model to multiple cities (Section 3.1.2).

3.1.1 Coupled Epidemic-Testing Single City Model. We first expand the standard four-state SEIR model to reflect reality better by considering different population groups (or compartments).

Population Groups/Compartments. The model distinguishes individuals into five population groups: susceptible, infected symptomatic, infected asymptomatic, and symptomatic but not COVID-19 infected (flu or general sick), and falsely presumed susceptible:

- We define *susceptible* as the population that is non-infected and displaying no symptoms associated with COVID-19.
- *Infected symptomatic* and *asymptomatic* are the sections of the population infected with COVID-19 who are showing symptoms and not exhibiting symptoms, respectively.
- *Symptomatic but not infected* are the people who are displaying symptoms (flu, general sick) similar to COVID-19, but are not infected.
- *Falsely presumed susceptible population* consists of people who have immunity from natural recovery, but erroneously test negative to COVID-19 antibodies.

As with the standard SEIR model, an individual enters and leaves these compartments according to the relevant transition rates and other parameters (Table 1). Different from the traditional set of dynamical equations, these transition

rates are governed by four different processes: (a) asymptomatic testing, (b) symptomatic testing, (c) immunization, and (d) falsely presumed susceptible process (Figure 2).

Exposure Dynamics. The exposure process is governed by the following equations:

$$\frac{dE}{dt} = \Big(\beta \cdot S(t) + \beta^{'} \cdot FPI(t)\Big) \cdot \frac{Infected(t)}{N} - \Big(per_a + per_s\Big) \cdot E(t) \tag{1}$$

where the total number of infected individuals at time t is,

$$Infected(t) = r \cdot \Big(PS(t) + PA(t) + IA(t) + ATN(t)\Big) + IS(t) + STN(t). \tag{2}$$

Above, the infection rate parameter, β, represents the number of new daily infection produced by a single infectious individual and it is equivalent to the product of contact rate and disease transmission rate. Equivalently, the total number of new infected individuals will be $\beta \cdot Infected(t) \cdot \frac{S(t)}{N}$, and this population will move from susceptible to exposed, where N denotes the total population. The parameter, $\beta^{'}$, represents a higher infection rate parameter, which we apply to the falsely presumed immune individuals (FPI) (i.e., individuals that falsely test positive to antibodies). More specifically, FPI is a recovered individuals that falsely tests positive for the serology, his/her risk is higher since the individual will likely behave in the assumption of larger than actual protection. Finally, equation (2) shows that asymptomatic individuals (IA(t) and ATN(t)) and individuals before symptom onset (PA(t), PS(t)) infect at r times the rate compared to symptomatic individuals.

Asymptomatic Testing Process. The *asymptomatic testing process* emulates random testing to discriminate infected asymptomatic from the susceptible population. The asymptomatic population is divided into two groups, *infected asymptomatic* and *not infected (susceptible)*. In practice, we cannot differentiate among these two groups of individuals without testing. Table 2 lists the sub-compartments relevant for the following equations that describe the asymptomatic testing process:

Table 2. Sub-compartments relevant for the asymptomatic testing process

Sub-Compartment		Sub-Compartment	
S	Susceptible population	E	Pop. exposed to the virus
PA	Pre-asymptomatic population	IA	Infected pop. who are asymptomatic
AT_i	Asymp. pop. receiving diagnostic test i	ATN	Asymptomatic pop. with negative test result
QAP	Asymp. pop. quarantined after a test	UR	Pop. with unknown immunity due to unknown infection
KR	Pop. of known recovered individuals	NT_i	Susceptible pop. receiving diagnostic test i
NTN	Pop. of non-infected indiv. who test negative	NTQ	Non-infected pop. quarantined due to testing error
FPI	Pop. of indiv. falsely presumed immune	PS	Infected pop. who are pre-symptomatic
IS	Infected pop. who are symptomatic	STN	Symptomatic pop. who test negative (by error)

An individual exposed to the virus will proceed as an infected asymptomatic individual with per_a rate; the virus will take η days for incubatation (during which the individual will be considered pre-asymptomatic) and after that period the individual will be considered infected asymptomatic (assuming that s/he does not show symptoms):

$$\frac{dPA}{dt} = per_a \cdot E(t) - PA(t - \eta) \tag{3}$$

If a government implements a random test for the asymptomatic population, ϕ_{ai} rate of IA(t) individuals get tested with test types i.

$$\frac{dIA}{dt} = PA(t-\eta) + ATN(t) - \sum_{i=1}^{2} \phi_{ai} \cdot IA(t) - \lambda \cdot IA(t) \tag{4}$$

Above, we assume that the λ is the rate of IA(t) individuals recover naturally:

$$\frac{dUR}{dt} = \lambda \cdot IA(t) + \lambda \cdot IS(t) - UR(t) \tag{5}$$

The following equation models impact of the sensitivity, tp_i, and the response time, τ_i, of test type i:

$$\frac{dAT_i}{dt} = \phi_{ai} \cdot IA(t) - tp_i \cdot AT(t-\tau_i) - (1-tp_i) \cdot AT(t-\tau_i) \tag{6}$$

The specificity, tn_i, of the test impacts the false positive rate for the test:

$$\frac{dNTN}{dt} = \sum_{i=1}^{2} (1-tn_i) \cdot NT_i(t-\tau_i) - NTN(t) \tag{7}$$

Once testing positive, the individual is quarantined for λ_q days, until recovering:

$$\frac{dQAP}{dt} = \sum_{i=1}^{2} tp_i \cdot AT(t-\tau_i) - QAP(t-\lambda_q) \tag{8}$$

$$\frac{dKR}{dt} = QAP(t-\lambda_q) + FSQ(t-\lambda_q) + QSP(t-\lambda_q) + \sum_{i=1}^{2} tn_1 \cdot HT_i(t-\tau_i) \tag{9}$$

Otherwise, the individual will move back to IA(t):

$$\frac{dATN}{dt} = \sum_{i=1}^{2} (1-tp_i) \cdot AT(t-\tau_i) - ATN(t) \tag{10}$$

Since we cannot distinguish an infected asymptomatic and a susceptible one, random tests are being employed not only for the infected asymptomatic but also for the susceptible ones:

$$\frac{dNT_i}{dt} = \phi_{ai} \cdot S(t) - tn_i \cdot NT_i(t-\tau_i) - (1-tn_i) \cdot NT_i(t-\tau_i) \tag{11}$$

If a test result is falsely positive, a non infected susceptible individual will be falsely quarantined for λ_q days:

$$\frac{dNTQ}{dt} = \sum_{i=1}^{2} tn_i \cdot NT_i(t-\tau_i) - NTQ(t-\lambda_q) \tag{12}$$

Otherwise, the tested individual moves to the susceptible compartment again

Table 3. Sub-Compartments relevant for the symptomatic testing process

Sub-Compartment		Sub-Compartment	
E	Pop. exposed to the virus	PS	Pre-Symptomatic population
IS	Infected pop. who are symptomatic	ST_i	Symptomatic pop. receiving test i
STN	Symptomatic pop. with negative test result	QSP	Symp. pop. quarantined after a test
UR	Pop. with unknown immunity due to unknown infection	KR	Pop. of known recovered individuals
$H1$	Pop. need hospitalization before a quarantine	$H2$	Pop. need hospitalization during quarantine
HT_i	Pop receiving test i while hospitalized	D	Pop. who have not recovered from the infection (dead)
FS	Pop. showing flu symptoms	FT_i	Pop. with flu symptom receiving test i
FTN	Pop. with flu symptom tested negative for COVID-19	FTQ	Pop. with flu symptom quarantined due to false positive
GS	Pop. with other COVID-like symptoms	GT_i	Pop. with other COVID-like symptoms reciving test i
GTN	Pop. with other symptoms tested negative for COVID-19	GTQ	Pop. with other symptoms quarantined due to false positive

Symptomatic Testing Process. The symptomatic testing process is designed to model the testing process for individuals who show COVID-19 like symptoms. We categorize symptomatic individuals into three populations: (a) COVID-infected symptomatic, (b) general sick (fever, coughing), and (c) flu symptomatic. We assume that these populations can be distinguished through diagnostic testing.

Much like the asymptomatic process discussed above, the process consists of testing, isolation, and quarantine sub-processes. Unlike the asymptomatic process, however, the symptomatic process also includes hospitalization and death for severe cases. The compartments presented in Table 3 along with the following differential equations define the transitions between relevant states in the symptomatic process.

An individual exposed to the virus will proceed as an infected symptomatic individual with per_s rate; the virus will take η days for incubatation (during which the patient is pre-symptomatic) and after that period the individual will be considered infected symptomatic (assuming that s/he does show symptoms):

$$\frac{dPS}{dt} = per_s \cdot E(t) - PS(t-\eta) \tag{13}$$

When the diagnostic tests are implemented for the symptomatic population, ϕ_{si} rate of infected symptomatic(IS(t)) individual get tested with test types i. Additionally, we assume that λ rate of IS(t) individuals recover naturally, and κ and h rates of IS(t) individuals are dead and hospitalized with the severe cases, respectively:

$$\frac{dIS}{dt} = PS(t-\eta) + STN(t) - \sum_{i=1}^{2} \phi_{si} \cdot IS(t) - \lambda \cdot IS(t) - \kappa \cdot IS(t) - h \cdot IS(t) \tag{14}$$

In the following equation, tp_i is sensitivity, and τ_i, represents response time of test types i.

$$\frac{dST_i}{dt} = \phi_{si} \cdot IS(t) - tp_i \cdot ST_i(t-\tau_i) - (1-tp_i) \cdot ST_i(t-\tau_i) \tag{15}$$

Once testing positive, the individual is quarantined for λ_q days until recovery, as shown in equations (6) and (12).

$$\frac{dQSP}{dt} = \sum_{i=1}^{2} tp_1 \cdot ST_i(t-\tau_i) - QSP(t-\lambda_q) \tag{16}$$

$$\frac{dKR}{dt} = QAP(t-\lambda_q) + FSQ(t-\lambda_q) + QSP(t-\lambda_q) + \sum_{i=1}^{2} tn_i \cdot HT_i(t-\tau_i) \tag{17}$$

Otherwise, the individual moves back to IS(t) and will contribute to the virus spread:

$$\frac{dSTN}{dt} = \sum_{i=1}^{2}(1-tp_i)\cdot ST_i(t-\tau_i) - STN(t) \tag{18}$$

Assuming that λ is the rate with which infected individuals recover from the disease and are (naturally) immunized, we have:

$$\frac{dUR}{dt} = \lambda \cdot IA(t) + \lambda \cdot IS(t) - UR(t) \tag{19}$$

Here, h is the rate with which individuals who were quarantined with positive test results (QSP(t)) move to the hospital. The death rate for hospitalized individuals is κ_h. After spending λ_h days in the hospital, the hospitalized individuals will take a test to check if the virus is still active and they will keep being hospitalized when the result is positive. Otherwise, they move to the recovered compartment as described in Equation 17.

$$\frac{dH1}{dt} = h \cdot QSP(t-\lambda_h) + (1-tn_1)\cdot HT1(t-\tau_1) - \kappa_h \cdot H1(t) \tag{20}$$

$$\frac{dH2}{dt} = h \cdot IS(t-\lambda_h) + (1-tn_1)\cdot HT2(t-\tau_1) - \kappa_h \cdot H2(t) \tag{21}$$

$$\frac{dHT_i}{dt} = \cdot H_i(t-\lambda_h) + (1-tn_i)\cdot HT_i(t-\tau_i) + tn_i \cdot HT_i(t-\tau_i) \tag{22}$$

$$\frac{dD}{dt} = \sum_{i=1}^{2} \kappa_h \cdot H_i(t) + \kappa \cdot QSP(t) + \kappa \cdot IS(t) \tag{23}$$

The following two equations leverage the flu and g_{sick} rate parameters to describe the portion of the population which show flu-like and general sick symptoms, such as fever and coughing, which require testing due to having symptoms indistinguishable from COVID-19.

$$\frac{dFS}{dt} = flu \cdot S(t) - FS(t) \tag{24}$$

$$\frac{dGS}{dt} = g_{sick} \cdot S(t) - GS(t) \tag{25}$$

Even though these individuals are not COVID-19 infected, in the case of a false positive, they will be quarantined for λ_q days:

$$\frac{dFT_i}{dt} = \phi_{si} \cdot FS(t) - tn_i \cdot FT_i(t-\tau_i) - (1-tn_i)\cdot FT_i(t-\tau_i) \tag{26}$$

$$\frac{dFTQ}{dt} = \sum_{i=1}^{2} tn_i \cdot NT_i(t-\tau_i) - FTQ(t-\lambda_q) \tag{27}$$

$$\frac{dGT_i}{dt} = \phi_{si} \cdot GS(t) - tn_i \cdot GT_i(t-\tau_i) - (1-tn_i)\cdot GT_i(t-\tau_i) \tag{28}$$

Table 4. Sub-compartments relevant for the process through which individuals obtain immunity

Sub-Compartment		Sub-Compartment	
KR	Pop. of known recovered indiviudals	*IM*	Pop. of individuals with immunity
STI	Pop. of immune indiv. receving serology (anti-body) test	*SII*	Pop. of not-immune indiv. receiving serology test
FPI	Pop. of individuals who are falsely presumed being immune		

$$\frac{dGTQ}{dt} = \sum_{i=1}^{2} tn_i \cdot GT_i(t-\tau_i) - GTQ(t-\lambda_q) \tag{29}$$

Patients who are true negative return to the susceptible population:

$$\frac{dGTN}{dt} = \sum_{i=1}^{2} (1-tn_i) \cdot GT_i(t-\tau_i) - GTN(t) \tag{30}$$

$$\frac{dFTN}{dt} = \sum_{i=1}^{2} (1-tn_i) \cdot FT_i(t-\tau_i) - FTN(t) \tag{31}$$

Immunity Process. The role of the immunity process is to model how individuals who recover from COVID-19 obtain immunity against reinfection for a certain period of time. This model is governed with sub-compartments presented in Table 4 along with the following equations:

Any person who recovers from the disease (KR(t)), will have immunity for γ days.

$$\frac{dIM}{dt} = KR(t) - IM(t-\gamma) - \phi_{se} \cdot IM(t) + tp_{se} \cdot STI(t-\tau_{se}) \tag{32}$$

In the above equation, the recovered individuals are divided into two groups: (a) individuals having immunity and those who do not get sufficient immunity. We assume that the government will administer serology tests at a predetermined rate,ϕ_{se}, for both groups, IM(t) & FPI(t), since we cannot discriminate an individual having immunity from those who lost immunity without a serology test. These tests are imperfect, much like the diagnostic tests. We use accuracy of tp_{se} and tn_{se} for sensitivity and specificity, respectively. The test takes τ_{se} days to provide the result:

$$\frac{dSTI}{dt} = \phi_{se} \cdot IM(t) - tp_{se} \cdot STI(t-\tau_{se}) - (1-tp_{se}) \cdot STI(t-\tau_{se}) \tag{33}$$

$$\frac{dSII}{dt} = \phi_{se} \cdot FPI(t) - tn_{se} \cdot FPI(t-\tau_{se}) - (1-tn_{se}) \cdot FPI(t-\tau_{se}) \tag{34}$$

Note that a group of individuals may be Falsely Presumed Immune (FPI(t)) for various reasons: (a) the individual may lose immunity (IM(t-γ)), (b,c) some individuals may be quarantined after false positive result with flu symptoms (FSQ(t-λ_q), after a general sickness (GSQ(t-λ_q)), or (d) after a testing error ((NTQ(t-λ_q)).

$$\frac{dFPI}{dt} = IM(t-\gamma) + GSQ(t-\lambda_q) + FSQ(t-\lambda_q) + NTQ(t-\lambda_q) - \beta' \cdot FPI(t) \tag{35}$$

For these individuals, we apply higher infection rate ($\beta' > \beta$), because these individuals are likely to socialize more than pure susceptible ones.

Table 5. Sub-compartments relevant for individuals who are falsely presumed susceptible

Sub-Compartment		Sub-Compartment	
UR	Pop. with unknown immunity due to unknown infection	FPS	Pop. falsely presumed susceptible
FST_i	Pop. falsely presumed susceptible receiving diag. test i	$FSTN$	Pop. falsely presumed susceptible who test negative
FSQ	Pop. falsely presumed susceptible (wrongly) quarantined		

Falsely Presumed Susceptible Process. The falsely presumed susceptible process is designed to consider those individuals recovered naturally from the COVID-19. These individuals have immunity against the disease, but they think themselves susceptible. In order to model this group of individuals, we consider the sub-compartments listed in Table 5, along with the following equations:

Unknown recovered individuals, who had COVID-19 but recovered naturally, have immunity against COVID-19:

$$\frac{dUR}{dt} = \lambda \cdot \Big(IA(t) + IS(t)\Big) - UR(t) \tag{36}$$

These individuals move to the falsely presume susceptible(FPS) since they regard themselves susceptible:

$$\frac{dFPS}{dt} = UR(t) + FSTN(t) + (1 - tp_{se}) \cdot STI(t - \tau_{se}) - FPS(t - \gamma) - \sum_{i=1}^{2} \phi_{ai} \cdot FPS(t) \tag{37}$$

Note that these individuals will lose immunity after γ days and move to the pure susceptible compartment.

While they are falsely presumed susceptible, these individuals will be subject to regular random testing strategies:

$$\frac{dFST_i}{dt} = \phi_{ai} \cdot FPS(t) - tn_i \cdot FST_i(t - \tau_i) - (1 - tn_i) \cdot FST_i(t - \tau_i) \tag{38}$$

$$\frac{FSTN}{dt} = \sum_{i=1}^{2} (1 - tn_i) \cdot FST1(t - \tau_i) - FSTN(t) \tag{39}$$

$$\frac{dFSQ}{dt} = \sum_{i=1}^{2} tn_i \cdot FST_i(t - \tau_i) - FSQ(t - \lambda_q) \tag{40}$$

As we see above, if the test is falsely positive, individuals are quarantined for λ_q days. Otherwise, they stay in FPS(t).

3.1.2 Spatially Informed SIRTEM Model. We note that the coupled epidemic/testing model described so far is not spatially informed. In particular, it assumes one group of individuals, whose interactions are defined through a single mixing rate. Moreover, the model further ignores the possibility of different geographic locations applying different testing policies. To account for these, we therefore extend the model with spatially indexed compartments along with spatially informed parameters and mixing rates. Let $\mathcal{S} = \{s_1, \ldots, s_M\}$ be a set of spatial locations.

- *Spatially indexed model compartments:* Tables 2 through 5 list the compartments of the base model. In the spatially informed model, each of these components are spatially indexed: for example, each spatial location s_i has a corresponding *susceptible* population, $S_{(i)}$, and an *exposed* population $E_{(i)}$.
- *Spatially informed mixing rates:* The infection rate parameter, β, in Table 1 includes two components: transmission rate, which (ignoring the local mutations of the disease) is a spatially-insensitive parameter, and the contact/mixing

Table 6. Average daily interactions per day per person in different contexts during different waves of the epidemic [25]

	Start	End	Work	Home	Other
Wave 0	22-Mar-20	9-Apr-20	0.25	2	0
Wave 1	10-Apr-20	4-May-20	0.5	2	1
–	5-May-20	16-Jun-20	0.625	2	1
Wave 2	17-Jun-20	23-Jun-20	0.75	2	1
–	24-Jun-20	10-Sep-20	1	2	1.5
Wave 3	11-Sep-20	26-Sep-20	1.25	2	2

rate, $\mu \in [0, 1]$, which depends on the behaviors of local populations, and therefore is spatial-sensitive:

$$\forall_{s_i \in \mathcal{S}} \;\; \beta_{(i)} = transmission\_rate \times \mu_{(i)}.$$

Here μ is the likelihood of each individual in the population to interact with other individuals in the same population.

The above equation, however, would fail to take into account potential mixing among spatially distributed population groups due to mobility patterns (such as daily commute between spatial regions). We, therefore, extend the above model as follows:

$$\forall_{s_i, s_j \in \mathcal{S}} \;\; \beta_{(i,j)} = transmission\_rate \times \mu_{(i,j)},$$

where $\mu_{(i,j)} \in [0, 1]$ denotes the likelihood of an individual in population at spatial location s_i to interact with an individuals in the spatial location s_j. Consequently, $\beta_{(i,j)}$ models the transmission of the disease from the from one population to another due to the underlying mobility patterns. We, therefore, revise the part of the model that governs the exposure process as follows:

$$\frac{dE_{(i)}}{dt} = \left(\sum_{s_j \in \mathcal{S}} \left(\beta_{(i,j)} \cdot S_{(i)}(t) + \beta'_{(i,j)} \cdot FPI_{(i)}(t) \right) \cdot Infected_{(j)}(t) \right) - \left(per_a + per_s \right) \cdot E_{(i)}(t)$$

where

$$Infected_{(i)}(t) = r \cdot \left(PS_{(i)}(t) + IA_{(i)}(t) + PA(t) + ATN_{(i)}(t) \right) + IS_{(i)}(t) + STN_{(i)}(t).$$

Above, as described earlier, the parameter, β', represents the larger infection coefficient that applies to the falsely presumed immunity individuals who potentially have large mixing rates than the susceptible population. The value of r in contrast takes into account the fact that the $transmission\_rate$ parameter is lower for asymptomatic and pre-symptomatic individuals than the fully symptomatic individuals.

Obtaining the Mixing Rates. In this paper, we obtain the mixing rate $\mu_(i, j)$ relying on two distinct information sources: [25] provides the rate with which people interact with other at home, work, and other activities during the COVID-19 pandemic. More specifically, this data source provides data about how the number of interactions per day per person changed over time during different waves of the epidemic 6. While this data does not include any spatial differentiation, we combine this data with the work commute data available at [11] to partition the mixing rate into to

three spatially differentiated components:

$$\mu(i,j) = h_{(i,j)} + w_{(i,j)} + o_{(i,j)},$$

where $h_{(i,j)}$ is the rate with which infected individuals in city i interact with susceptible people in city j in the *home* context, $w_{(i,j)}$ is the rate with which infected individuals in city i interact with susceptible people in city j in the *work* context, and $o_{(i,j)}$ is the rate with which infected individuals in city j interact with susceptible people in city i in all *other* contexts:

- *At-home mixing:* In order to compute the rate of interactions in the home context, we make the simplifying assumption that, at home, individuals only interact with those individuals living in the same city; i.e.,

  $$h_{(i,j)} = \varnothing \quad if \quad i \neq j.$$

  Given this assumption, we can obtain the *at-home* mixing rate, $h_{(i,i)}$, at city i as

  $$h_{(i,i)} = \frac{num\_home\_interaction}{pop_i},$$

  where $num\_home\_interaction$ is the number of per day, per person at-home interactions reported in Table 6 and pop_i is the population of the city i.
- *At-work mixing:* In order to compute the rate of interactions in the work context, we rely on the commute rate data available from [11]. More specifically,

  $$w_{(i,j)} = \left(\frac{num\_work\_interactions}{pop_j} \times \frac{W_{j\to i}}{W_j}\right) + \left(\frac{num\_work\_interactions}{pop_i} \times \frac{W_{i\to j}}{\sum_h W_{h\to j}}\right).$$

  Above, the first term indicates the interaction rate due to individuals traveling from city j to city i for work related reasons: more specifically, W_j is the number of workers living in city j and $W_{j\to i}$ is the number of those that commute to city i for work.

  The second term, on the other hand, is the interaction rate due to individuals traveling from city i to city j for work: $W_{i\to j}$ is the number of people that commute from city i to city j for work, while $\sum_h W_{h\to j}$ is the number of individuals working in city j.
- *Other mixing:* To obtain non-home, non-work mixing rates, we assume that the rate interaction among individuals is inversely proportional with the square of their distance; i.e.,

  $$o_{(i,j)} = \frac{num\_other\_interactions}{pop_i} \times \frac{Z_{(i,j)}}{\sum_h Z_{(h,j)}},$$

  where $num\_other\_interaction$ is the number of non-home, non-work related interactions reported in Table 6 and $Z_{(i,j)}$ is the population of city i normalized with the square of the distance between cities i and j:

  $$Z_{(i,j)} = \frac{pop_i}{\delta^2_{(i,j)}}.$$

  We obtained the distance $\delta_{(i,j)}$ between cities i and j from [48] and approximated $\delta_{(i,i)}$ as $min_h\left(\delta_{(i,h)}\right)/2$.

3.2 Optimal Testing

We use the epidemic/testing model, SIRTEM, to develop an optimization problem for identifying optimal testing strategies: The objective of the problem P is to minimize the total economic cost, consisting of testing (f_1), hospitalization (f_2), and

quarantine (f_3) costs, of the COVID-19, subject to resource (testing and hospital capacity) limitations. At each time frame t, We apply rolling horizon optimization formulation(one time frame look ahead) to prevent locally optimized solution at each time frame as following:

$$P_t: \quad \min_{x=(\omega_t,\omega_{t+1})} z_t^o = \sum_{k=1}^{3} (f_k^t(\omega_t) + f_k^{t+1}(\omega_{t+1})) \tag{41}$$

s.to

$$Z_{1,d}^c: \quad g_d^{T1}(\omega(t)) \leqslant T1 \qquad \forall d \in \mathcal{D}(t) \tag{42}$$

$$Z_{2,d}^c: \quad g_d^{T1}(\omega(t+1)) \leqslant T1 \qquad \forall d \in \mathcal{D}(t+1) \tag{43}$$

$$Z_{3,d}^c: \quad g_d^{T2}(\omega(t)) \leqslant T2 \qquad \forall d \in \mathcal{D}(t) \tag{44}$$

$$Z_{4,d}^c: \quad g_d^{T2}(\omega(t+1)) \leqslant T2 \qquad \forall d \in \mathcal{D}(t+1) \tag{45}$$

$$Z_{5,d}^c: \quad H_d(\omega_t) \leqslant H \qquad \forall d \in \mathcal{D}(t) \tag{46}$$

$$Z_{6,d}^c: \quad H_d(\omega_{t+1}) \leqslant H \qquad \forall d \in \mathcal{D}(t+1), \tag{47}$$

The optimization problem P_t, is solved in a rolling horizon manner for $t = 1, \ldots, T-1$ using a lookahead of one time period. Herein, a time period t refers to a month, while d is day, and the set $\mathcal{D}(t)$ represents the number of days in month t. At each time period t, we choose the testing rates to apply. Therefore, the decision variables $\omega_t = (\phi_{a1}^t, \phi_{a2}^t, \phi_{s1}^t, \phi_{s2}^t)$, where $(\phi_{a1}^t, \phi_{a2}^t, \phi_{s1}^t, \phi_{s2}^t)$ represent daily asymptomatic and symptomatic testing rate for test type 1 and 2 in time period t. These decision variables are real numbers in the range of [0,1]. The objective in (41), together with the constraints in equations (42)-(47) are blackbox functions and, therefore, they require simulation to be evaluated. Specifically, g_d^{T1}, g_d^{T2}, represent the daily total number of tests of type 1 and 2 administered, respectively, to be compared to the total daily testing capacity T_1,T_2. There are $\mathcal{D}(t)$ of these constraints for each month t, and for each test type. in constraints (46)-(47), H_d denotes the hospital beds used daily, to be compared to the daily available hospital bed capacity, H. There are $\mathcal{D}(t)$ of these constraints for each time period t.

We used a Constrained Bayesian optimization with rolling horizon approach to solve the given problem. The sampling algorithm was taken from [27], and it is reported as Step 1 in Algorithm 1, below.

Algorithm 1: Bayesian Optimization for Optimal Testing.

Result: $\{\omega_t^*\}_{t=1}^T = \{(\phi_{a1}^*, \phi_{a2}^*, \phi_{s1}^*, \phi_{s2}^*) \subset R^4\}_{t=1}^T$

Input: Decision space $\Omega \subset \mathbb{R}^8$, hospital bed limit H, maximum number of daily tests for test type 1 and 2, $(T1, T2)$, number of initial sample n_0, total budget B;

for $t < T - 1$ **do**

Initialization:

Best value so far $\tilde{Z}_t^{*,o} \leftarrow \infty$, set of sampled points $S_0^t \leftarrow \varnothing$;

Sample n_0 locations $\left\{x_t^\tau = \left(\omega_t^\tau, \omega_{t+1}^\tau\right)\right\}_{\tau=1}^{n_0}, S_0^t \leftarrow S_0^t \cup \left\{x_t^\tau = \left(\omega_t^\tau, \omega_{t+1}^\tau\right)\right\}_{\tau=1}^{n_0}$;

for $\tau = 1, \ldots, n_0$ **do**

Run SIRTEM and evaluate the objective function $z^o\left(x_t^\tau\right)$ in eqn. (41), and the constraints $z_{r,t}^c\left(x_t^\tau\right), r = 1, \ldots, R$ from eqn. (42)-(47);

if $z^o\left(x_t^\tau\right) < \tilde{Z}_t^*$, *and* x_t^τ *is feasible* **then**

$\tilde{Z}_t^* \leftarrow x_t^\tau, \tilde{x}_t^* = x_t^\tau$;

end

end

Estimate a Gaussian process model for the objective and the constraints:

$Z_t^o \sim GP\left(\mu^o\left(x_t\right), s^{2,o}\left(x_t\right) \mid \left\{x_t^\tau, z^o\left(x_t^\tau\right)\right\}_{\tau=1}^{n_0}\right)$, obtain the predictor $\hat{Z}^o\left(x_t\right), \forall x_t$;

$Z_{r,t}^c \sim GP\left(\mu_r^c\left(x_t\right), s_r^{2,c}\left(x_t\right) \mid \left\{x_t^\tau, z_r^c\left(x_t^\tau\right)\right\}_{\tau=1}^{n_0}\right)$, obtain the predictor $\hat{Z}_r^c\left(x_t\right), \forall x_t, r = 1, \ldots, R$;

$b \leftarrow n_0 + 1$;

while $b \leqslant B$ **do**

Step 1: Sample $x_t^b \in \arg\max_{x_t} CEI\left(x_t\right) = EI\left(x_t\right) \cdot \prod_{r=1}^R \left[P\left(Z_r^c\left(x_t\right) \in C_r\right)\right]$, where $P\left(Z_r^c\left(x_t\right) \notin C_r\right)$ is the probability that the r^{th} constraint is violated, while $EI\left(x_t\right) = E\left[\max\left(0, \Delta_{Z^o}\left(x_t\right)\Phi\left(\frac{\Delta_{Z^o}(x_t)}{s^o(x_t)}\right) + s^o\left(x_t\right)\phi\left(\frac{\Delta_{Z^o}(x_t)}{s^o(x_t)}\right)\right)\right]$, and $\Delta_{Z^o}\left(x_t\right) = \tilde{Z}_t^* - \hat{Z}^o(x_t)$;

$S \leftarrow S \cup x_t^b$;

Step 3: Evaluation

Run SIRTEM and evaluate the objective function $z^o\left(x_t^b\right)$ in eqn. (41), and the constraints $z_{r,t}^c\left(x_t^b\right), r = 1, \ldots, R$ from eqn. (42)-(47);

if $z^o\left(x_t^b\right) < \tilde{Z}_t^*$, *and* x_t^b *is feasible* **then**

$\tilde{Z}_t^* \leftarrow x_t^b, \tilde{x}_t^* = x_t^b$;

end

Step 4: Models Update

$Z_t^o \sim GP\left(\mu^o\left(x_t\right), s^{2,o}\left(x_t\right) \mid \left\{x_t^\tau, z^o\left(x_t^\tau\right)\right\}_{\tau=1}^{b}\right)$, obtain the predictor $\hat{Z}^o\left(x_t\right), \forall x_t$;

$Z_{r,t}^c \sim GP\left(\mu_r^c\left(x_t\right), s_r^{2,c}\left(x_t\right) \mid \left\{x_t^\tau, z_r^c\left(x_t^\tau\right)\right\}_{\tau=1}^{b}\right)$, obtain the predictor $\hat{Z}_r^c\left(x_t\right), \forall x_t, r = 1, \ldots, R$;

$b \leftarrow b + 1$;

end

end

4 EVALUATION

4.1 Single City Model Validation

4.1.1 Parameter Calibration. For a given geographic location (this could be county, state, city), we calibrate the SIRTEM model by estimating three critical parameters, infection rate (β), testing rate (ϕ_s), and the general symptomatic rate (g) using published data of confirmed positive and negative cases (Table 7). We made the following assumptions:

- There is only one diagnostic test and one serology test available;
- Flu and general symptomatic-related compartments are collapsed into one, and the underlying rate (g) is assumed to be constant over time.

We obtain estimation of these three parameters by solving an Given the complexity of the simulator, we cannot optimize the likelihood in closed form. Instead, we defined an algorithm to iteratively improve the discrepancy between the daily positive and negative cases predicted against the real data.

$$(P) : \min_{\omega \in \Omega} Z(\omega) = \frac{1}{2}\left[\frac{\frac{1}{d}\sum_{t=1}^{d}(\hat{y}_t^{(+)}|\omega) - y_t^{(+)})^2)}{\bar{y}_t^{(+)}} + \frac{\frac{1}{d}\sum_{t=1}^{d}(\hat{y}_t^{(-)}|\omega) - y_t^{(-)})^2}{\bar{y}_t^{(-)}}\right] \tag{48}$$

In equation (48), $\hat{y}_t^{(+)}, \hat{y}_t^{(-)}$ are the SIRTEM predictions for positive and negative cases at time t (day), respectively. $y_t^{(+)}$, $y_t^{(-)}$ denote confirmed positive and negative cases obtained from public sources [61]. Each error term is normalized using the average confirmed cases, $\bar{y}_t^{(+)}$ and $\bar{y}_t^{(-)}$, respectively.

The changes of the two key parameters, the relative infection rate β, and the diagnostic testing rate ϕ (assuming only one test), over time to follow a functional form. More specifically, we assume both to be autoregressive, and we use an AR(2) model for their calibration. As a result, for each *week* k, we have:

$$\beta_k = a_1 \cdot \beta_{k-1} + a_2 \cdot \beta_2 + e_k^b \tag{49}$$

$$\phi_k = b_1 \cdot \phi_{k-1} + b_2 \cdot \phi_{k-2} + e_k^s \tag{50}$$

$$\forall_k \quad g_k = g. \tag{51}$$

Under these assumptions, the decision vector $\omega = [\mathbf{a}, \mathbf{b}, g]$, requiring to estimate $\mathbf{a}, \mathbf{b}$, both 2-dimensional vectors, and the parameter g. This results in a 5-dimensional decision problem, which we treat as a black box optimization, and use

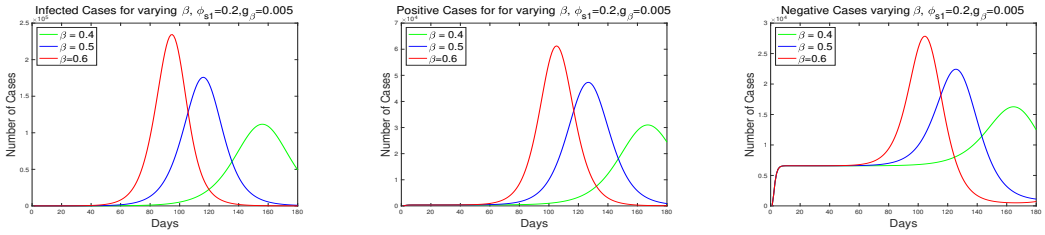

Fig. 3. Numbers of COVID-19 Infections and Positive and Negative test results for different values of β

K weeks of data to calibrate. Specifically, we designed an iterative procedure for the optimization of the autoregressive parameters in (49)-(50) and g. The approach is summarized in Algorithm 2.

Algorithm 2: Calibration Algorithm for $\mathbf{a}, \mathbf{b}, g$.

Result: 5 dimensional coefficient vector $\tilde{\omega}^* = \left(\tilde{\boldsymbol{a}}^*, \tilde{\boldsymbol{b}}^*, \tilde{g}^*\right) \in \mathbb{R}^5$ and $\tilde{\boldsymbol{\beta}}^*, \tilde{\boldsymbol{\phi}}^*$ using eqn. (49)-(50)

Initialize $\mathbf{a}^0 \subset \mathbb{R}^2, \mathbf{b}^0 \subset \mathbb{R}^2, g^0 \in \mathbb{R}, \tilde{Z}^* = \infty$

$h \leftarrow 1$;

Set $\mathbf{a}^h = \mathbf{a}^0, \mathbf{b}^h = \mathbf{b}^0, g^h = g^0$

while $h \leqslant H$ **do**

Step1 : Use AR(2) eqn. (49)-(50) to determine the SIRTEM parameters $\boldsymbol{\beta}(h), \boldsymbol{\phi}(h)$ from $\mathbf{a}^h, \mathbf{b}^h$;

Step2 : Run SIRTEM for K weeks and obtain the daily estimates $\left(\hat{y}_t^{(+)}, \hat{y}_t^{(-)}\right)_{t=1}^{K\times 7}$, use training data $\left(y_t^{(+)}, y_t^{(-)}\right)_{t=1}^{K\times 7}$ and calculate $Z(\omega^h)$ using eqn. (48);

Step 3: Update the incumbent;

if $Z(\omega^h) < \tilde{Z}^*$ **then**

$\tilde{\omega}^* \leftarrow \omega^h$;

$\tilde{Z}^* \leftarrow Z(\omega^h)$;

end

Step 3: Build the surrogate for the error function

$Z(\omega) \sim GP\left(\mu(\omega), s^2(\omega) \mid \{\omega^\tau = [\mathbf{a}^\tau, \mathbf{b}^\tau, g^\tau], z(\omega^\tau)\}_{\tau=1}^h\right)$ using Gaussian process regression (GP), and obtain the predictor $\widehat{Z}(\omega)$, $\forall \omega \in \Omega$;

Step 4: Sample the next location that maximizes the expected improvement (EI) given the predictor $\widehat{Z}$:

$\omega^{h+1} \in \arg\max_{\omega\in\Omega} EI\left(\widehat{Z}(\omega)\right) = E\left[\max\left(0, \Delta_Z(\omega)\,\Phi\left(\frac{\Delta_Z(\omega)}{s(\omega)}\right) + s(\omega)\,\phi\left(\frac{\Delta_Z(\omega)}{s(\omega)}\right)\right)\right]$, where

$\Delta_Z(\omega) = \tilde{Z}^* - \widehat{Z}(\omega)$;

$h \leftarrow h + 1$;

end

Table 7. Default values for various SIRTEM model parameters

Parameter	Description	Values	Reference
tp_1	Sensitivity of diagnostic test	0.75	[19, 72]
tn_1	Specificity of the diagnostic test	0.95	[72]
tp_{se}	Sensitivity of the serology test	0.84	[8]
tn_{se}	Specificity of the serology test	0.97	[8]
τ_1	Time to result for diagnostic test	3days	Assumption
τ_{se}	Time to result for the serology test	5days	Assumption
ϕ_1	Diagnostic testing rate for symptomatic individuals	Estimated	
ϕ_{a1}	Diagnostic testing rate for non-symptomatic individuals	0	Assumption
ϕ_{se}	Serology Test rate	0.01	Assumption
β	Infection rate for the susceptible pop.	Estimated	
β'	Inf. rate for falsely presumed immune pop. (ratio)	$1.2{\cdot}\beta$	Assumption
r	Ratio of transmission rates for asympt. population against sympt. population	0.51	[10]
per_a	Percentage of ind. with COVID-19 who are asymptomatic	0.16	[10]
per_s	Percentage of ind. with COVID-19 who are symptomatic	0.84	[10]
η	Incubation length (days)	3.2 days	[10]
λ_a	Length of recovery for asymptomatic ind. (days)	3.5 days	[10]
λ_s	Length of recovery for symptomatic ind. (days)	7 days	[10]
λ_q	Length of quarantine (days)	14 days	[14]
h	hospitalization rate (ratio of quarantined pop, per day)	0.06	[17]
λ_h	Hospitalization length (days)	6 days	[14]
κ	Mortality rate for symptomatic pop. (per day)	0.0088	[10]
κ_h	Mortality rate for hospitalized individuals (per day)	0.074	[17]
g	Ratio of susc. who have fever for non COVID infections (ratio, per day)	Estimated	

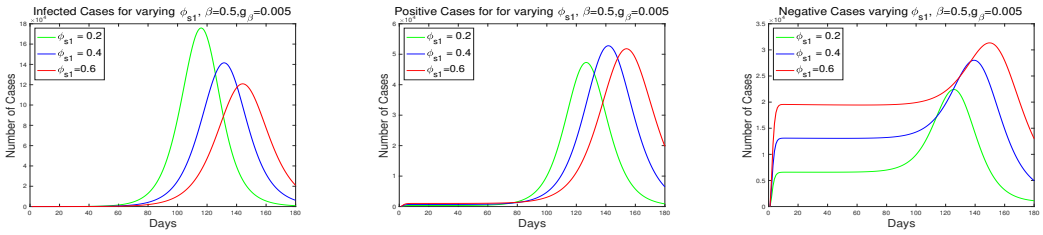

(a) (b) (c)

Fig. 4. Numbers of COVID-19 Infections, Positive and Negative test results for different values of ϕ_{s1}

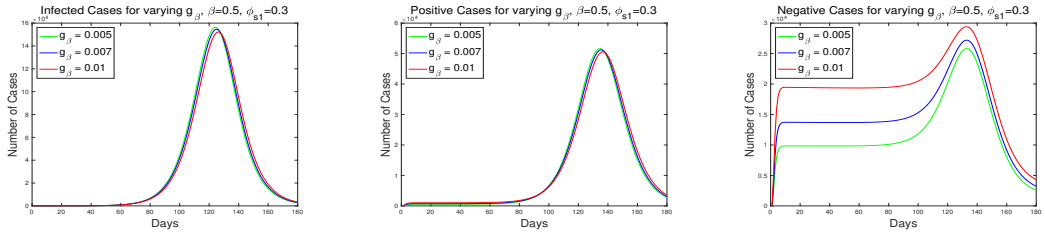

Fig. 5. Numbers of COVID-19 Infections, Positive and Negative cases for different values of g

Impact of the Model Parameters. Before considering specific US states, we investigate the impact of the various key model parameters on the progression of the COVID-19 epidemic. For this purpose, we consider a state with total population of 7 million and start the epidemic with 10 symptomatic and 10 asymptomatic individuals. We simulate the epidemic under 180 days.

Impact of β on COVID-19 Progression. Figure 3 shows how the infection rate, β affects the positive & negative cases. As expected, a higher infection rate, β, results in a larger number of COVID-19 infected individuals as shown in Figure 3(a). This in turn results in larger numbers of positive and negative test results as shown in Figures 3(b) and (c). Here, the increase in the negative cases is due to the imperfection in the diagnostic test.

Impact of ϕ_{s1} on COVID-19 Progression. A higher testing rate, ϕ_{s1}, would indicate that the authorities are actively trying to find COVID-19 infected individuals from the population, which is likely to increase positive test results. However, a strong testing campaign would decrease the infection itself, which in turn would push the positive test cases down. We study this complex relationship in Figure 4 (a). As we see in Figure 4(b), as a result of this, a higher testing rate is able to slow the epidemic progress but does not significantly impact the peak positive test results. Additionally, a higher testing rate also increases the number of negative test results for a fixed general sick rate, g (Figure 4(c)).

Impact of g on COVID-19 Progression. General sick rate, g, contributes to increased negative cases because a higher general sick rate means more individuals show symptoms (coughing, fever) but are not COVID-19 infected. As seen in Figure 5(c), the gap between the negative cases for different values of g diminishes after 110 days; this is largely due to significant drops in the false negative cases.

Table 8. Populations of the four states considered in the case study

State	Population
Arizona	7.3 million
Florida	21.5 million
Minnesota	5.6 million
Wisconsin	5.8 million

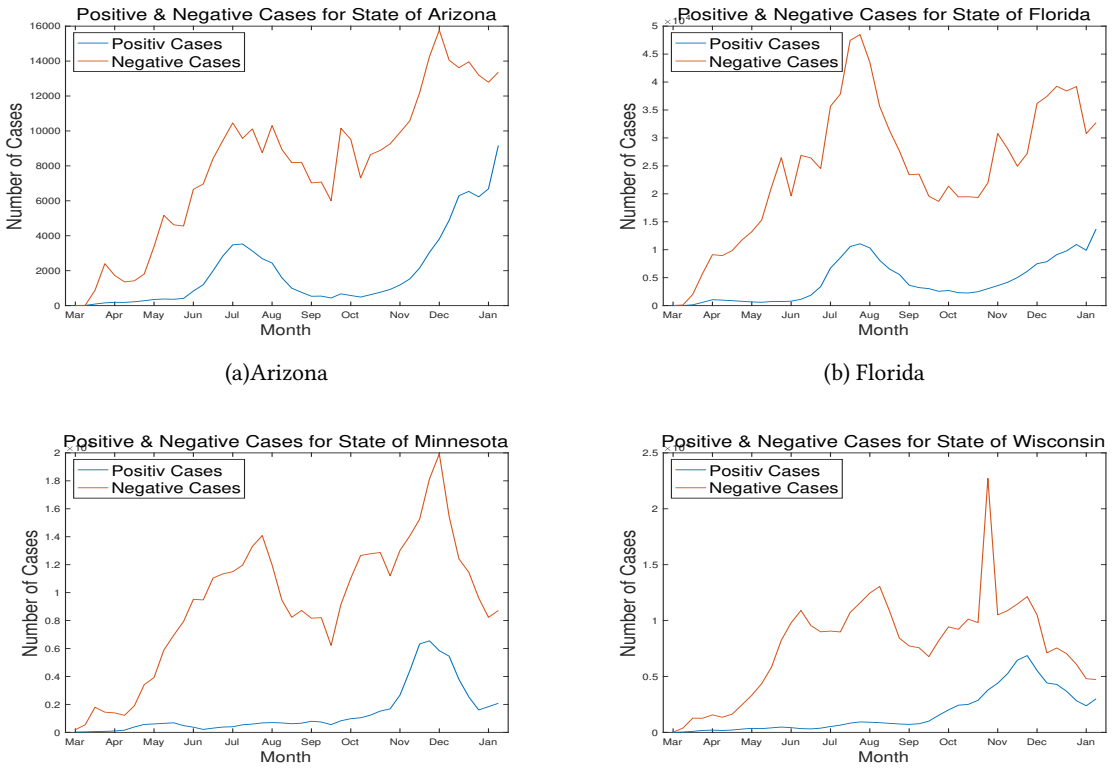

(a)Arizona (b) Florida

(c) Minnesota (d) Wisconsin

Fig. 6. Incidence numbers for 4 U.S. states

4.1.2 Case Studies with Four U.S. Cities. We next compare the prediction results of the proposed model with calibrated model parameters against the published confirmed case data for four U.S. states, Arizona, Florida, Wisconsin, and Minnesota. The model parameters are calibrated relying on the parameter values presented in Table 7 obtained from various sources, including recent research results and CDC published data. Table 8 and Figure 6 show the populations and the weekly moving averages of reported positive and negative cases of the four states considered in the case study [17].

Arizona and Florida have seen two waves of case growth during July and December. In contrast, Minnesota and Wisconsin kept the epidemic under control until September, but suffered from rapid growth of cases during the second wave of the pandemic in December 2020. We use these confirmed cases to calibrate the three key parameters of the epidemic for each state by solving the optimization problem reported in Section 4.1.1. The results are presented in Figure 7 and Table 9: as we see here, the model predicts the reported positive cases very accurately for the southern states, Arizona and Florida.

Table 9. Normalized mean squared error for the 4 U.S states

State	$\overline{y1}$	$\overline{y2}$	$\frac{\frac{1}{d}\sum_{t=1}^{d}(f1_t - y1_t)^2}{\overline{y1}}$	$\frac{\frac{1}{d}\sum_{t=1}^{d}(f2_t - y2_t)^2}{\overline{y2}}$	$\frac{1}{2}\left[\frac{\frac{1}{d}\sum_{t=1}^{d}(f1_t - y1_t)^2}{\overline{y1}} + \frac{\frac{1}{d}\sum_{t=1}^{d}(f2_t - y2_t)^2}{\overline{y2}}\right]$
Arizona	1937.1	7975.8	0.295	0.264	0.2797
Florida	4427.4	24559.4	0.3227	0.2185	0.2706
Wisconsin	1752.9	7738.8	0.325	0.343	0.334
Minnesota	1417.7	9222.6	0.5201	0.2305	0.3753

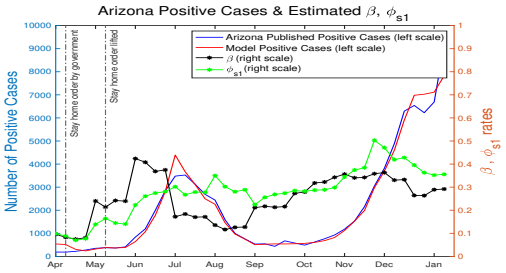

(a) Positive results in Arizona

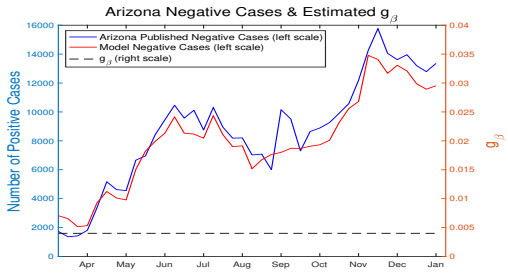

(b) Negative results in Arizona

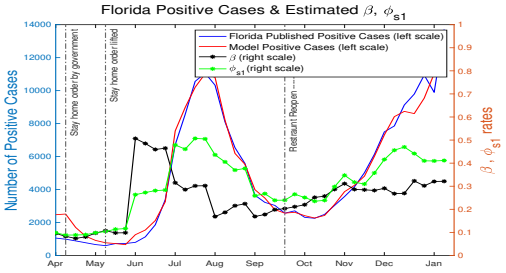

(c) Positive results in Florida

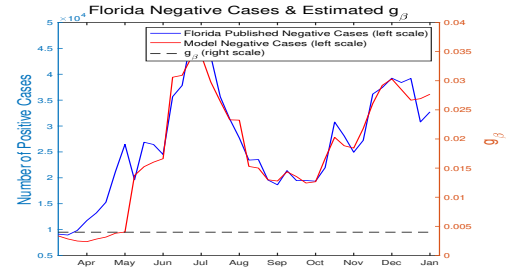

(d) Negative results in Florida

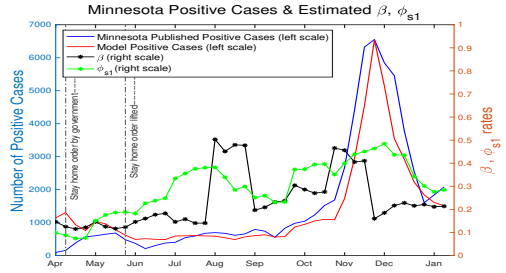

(e) Positive results in Minnesota

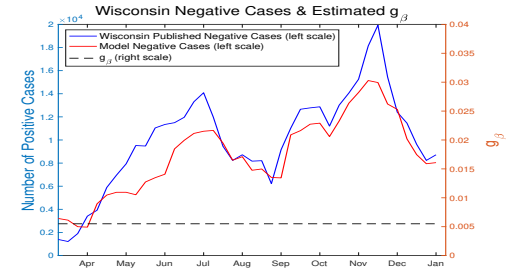

(f) Negative results in Minnesota

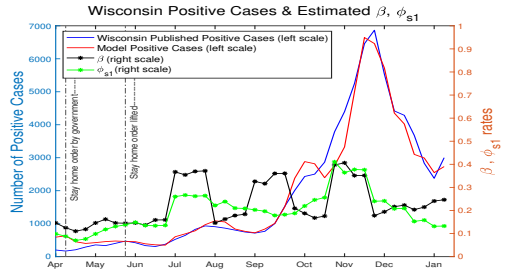

(g) Positive results in Wisconsin

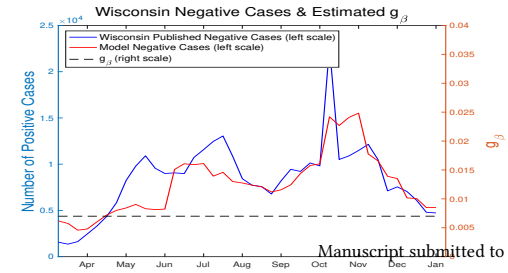

(h) Negative results in Wisconsin

Fig. 7. Model prediction results for the four U.S, states in this case study

The prediction, especially, for the negative test results is somewhat off for the northern states, Minnesota and Wisconsin. This is apparently because the general symptomatic rate was assumed to be constant through out the simulation, which may not be less a valid assumption for the colder states in the north.

As we see in Figures 7(a) and (c), in Arizona and Florida, the first major hike of the infection rate, β, follows soon after the governments' lifting of the stay-home orders in May. We see that while β dropped fast as people in these States panicked with the rapid increase of the positive case numbers, soon after the value of the β parameter started a slower but consistent creep up as the population started suffering from social distancing fatigue. The negative cases for these two states, reported in Figures 7(b) and (c), are also predicted quite accurately; in fact, they follow the the testing rates (reported in (Figures 7(a) and (b)) closely): the more testing done, the higher numbers of negative cases are reported.

In contrast to Arizona and Florida, Wisconsin and Minnesota managed the epidemic better until September. Unfortunately, the infection rate, β, in both of these states do see a rapid increase roughly 1 to 1.5 month after lifting of the stay home order, as seen in Figures 7(e) and (g). Similar to Arizona and Florida, the model negative cases (Figures 7(f) and (h)) follow the predicted testing rates; but the overall fit with the published negative cases is not as strong, presumably due to less stable general symptomatic rates in these two colder Northern states.

4.2 Optimal Testing Policies

In this section, we present the optimization result with single area model (i.e., $c = 1$) to investigate the relationship among testing policy, cost, and other parameters. In the results reported in this section, we consider various scenarios where two alternative tests, with different accuracies, are being deployed:

- *Test* #1: This is a relatively more accurate (high sensitivity, 0.75, and specificity, 0.95) test, with correspondingly high cost, \$50.
- *Test* #2: This is a cheaper and less accurate test. In particular, we varied test sensitivity between 0.50 and 0.75, specificity between 0.70 and 0.95, and cost between 1 and 50,

For the test problem setting, we sampled 50 cases of test set with latin hypercube sampling Detailed parameter values obtained through sampling are shown in the appendix. We note that the optimization problem is solved Bayesian Optimization technique with inequality constraint [27] More specifically, we considered a 10 month period, with the first 2 months marked as the "*early*", the last 2 months marked as the "*late*", and the middle 6 months marked as the "*active*" period of the epidemic. For each scenario, we have computed the cost optimal deployment strategy and in the rest of this section we present the key outcomes from this set of experiments.

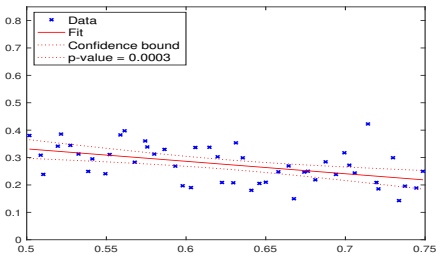

(a) Test 2 sensitivity vs. Test 1 rate

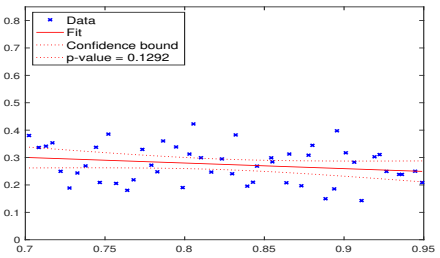

(b) Test 2 specificity vs. Test 1 rate

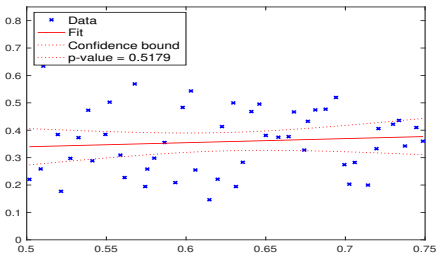

(c) Test 2 sensitivity vs. Test 2 rate

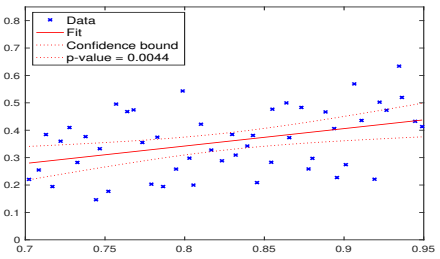

(d) Test 2 specificity vs. Test 2 rate

Fig. 8. The impact of the accuracy of the alternative test on the testing rates (X-axis: Accuracy; Y-Axis: Testing rate)

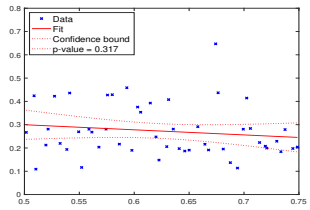

(a) Test 2 sens. vs. % Test 2 (early)

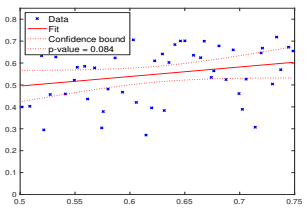

(b) Test 2 sens. vs. % Test 2 (active)

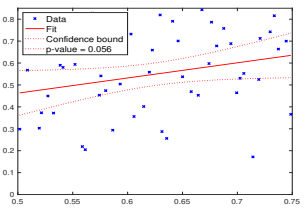

(c) Test 2 sens. vs. % Test 2 (late)

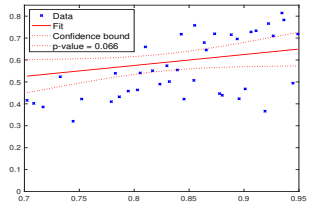

(d) Test 2 spec. vs. % Test 2 (early)

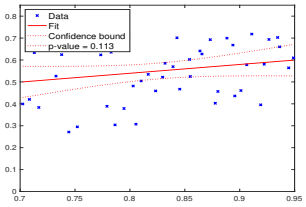

(e) Test 2 spec. vs. % Test 2 (active)

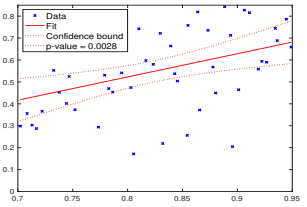

(f) Test 2 spec. vs. % Test 2 (late)

Fig. 9. The impact of accuracy of the alternative test on the testing rate trade-off at different phases of the epidemic (X-axis: Accuracy; Y-Axis: Testing rate)

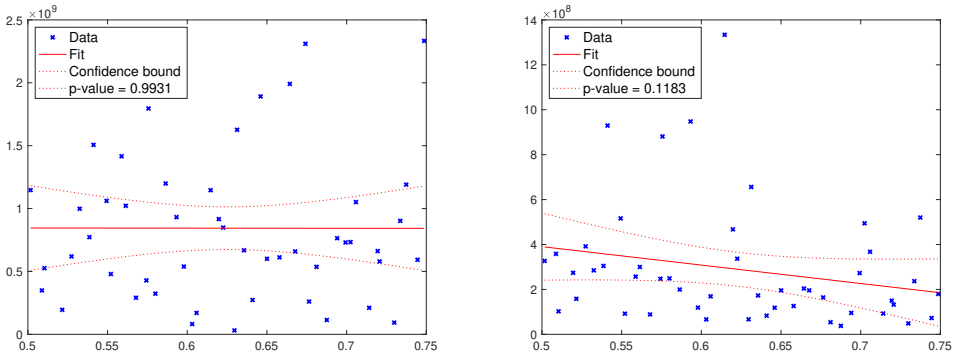

(a) Test 2 sensitivity vs. Quarantine cost. (b) Test 2 specificity vs. Quarantine cost.

Fig. 10. Impact of accuracy of the alternative test on the quarantine costs (X-axis: Accuracy; Y-Axis: Quarantine cost)

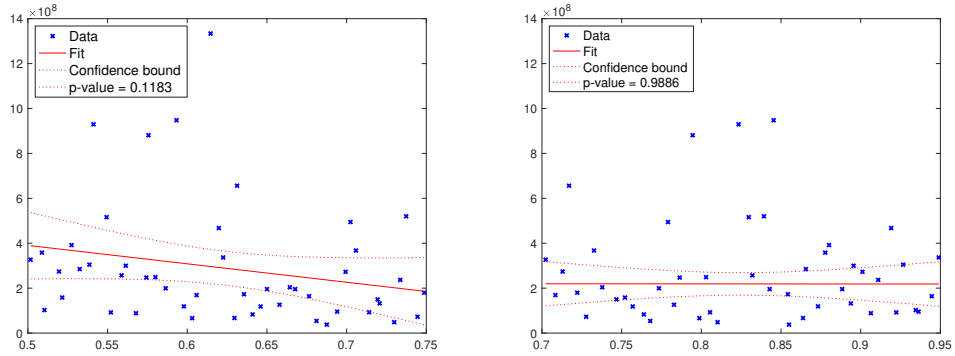

(a) Test 2 sensitivity vs. Hospitalization cost. (b) Test 2 specificity vs. Hospitalization cost.

Fig. 11. Impact of accuracy of the alternative test on hospitalization costs (X-axis: Accuracy; Y-Axis: Hospitalization cost)

Impact of Accuracy of the Alternative Test on the Testing Rates. In Figure 8, we plot four charts depicting the impact of the accuracy of the Test 2 on the testing rates for both Tests 1 and 2. As we see in Figures 8(a) and (b) as the accuracy of Test 2 increases, this translates into lesser use of Test 1 – considering that Test 2 is cheaper, this is expected. We also see in Figures 8(c) and (d) that as the accuracy of Test 2 increases, a larger portion of the population is tested with the cheaper test, Test 2. This result is also confirmed in Figure 9, where we see that the percentage of test of Type 2 increases with increasing sensitivity and selectivity during all phases of the epidemic.

Impact of Accuracy of the Alternative Test on the Quarantine and Hospitalization Rates. In Figures 10 and 11, we consider the impact of accuracy of the alternative test on the quarantine and hospitalization costs. As we see in Figures 10(a) and (b), the sensitivity of the Test 2 has only minimal impact on the quarantine costs; in contrast, improved specificity of Test 2 has a strong impact on reductions on the quarantine rates. As we see in Figure 11, on the other

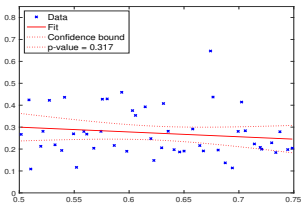

(a) Test 2 sens. vs. Asymp. tests (early)

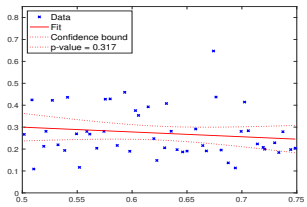

(b) Test 2 sens. vs. Asymp. tests (active)

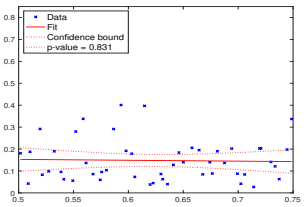

(c) Test 2 sens. vs. Asymp. tests (late)

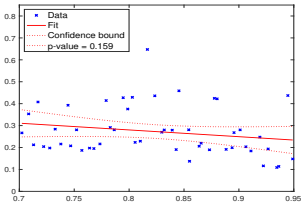

(a) Test 2 spec. vs. Asymp. tests (early)

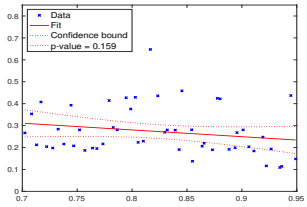

(b) Test 2 spec. vs. Asymp. tests (active)

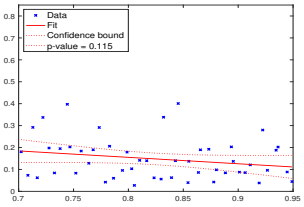

(c) Test 2 spec. vs. Asymp. tests (late)

Fig. 12. The impact of accuracy of the alternative test on the percentage of asymptomatic tests run

hand, the accuracy of Test 2 have almost no impact on the hospitalization (while more accurate (especially specific) tests tend to reduce the quarantine costs, the trend is quite weak as indicated by a large p-value).

Impact of the Accuracy of the Alternative Test on the Percentage of Asymptomatic Tests Run. As we see in Figures 12(a,b,c) if the cheaper test, Test 2, is highly sensitive, it raises the ratio of the symptomatic testing (as opposed to the asymptomatic testing) done during the early stages of the epidemic – the accuracy of the test, however, does not have an impact on the relative symptomatic vs. asymptomatic testing rates during the active and late stages if the epidemic. The specificity of Test 2 also promotes symptomatic testing as opposed to asymptomatic testing, but this time during both early and late phases of the epidemic – see Figures 12(d,e,f). Once again, during the active phase of the epidemic, the accuracy of the test does not have a significant impact on the balance of symptomatic vs. asymptomatic testing rates.

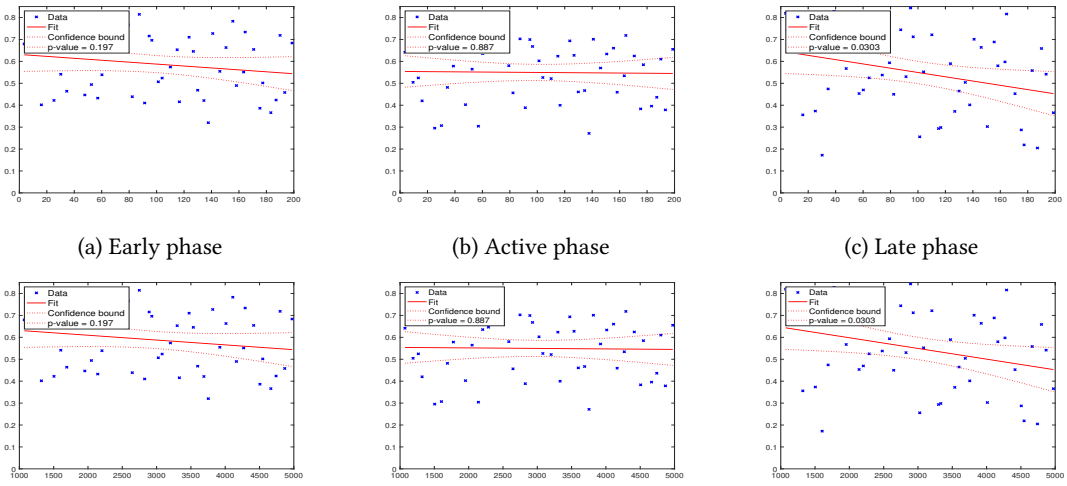

(a) Early phase (b) Active phase (c) Late phase

(d) Early phase (e) Active phase (f) Late phase

Fig. 13. The impact of (a,b,c) unit quarantine and (d,e,f) hospitalization costs on the choice of Test 2

Impact of the Unit Quarantine and Hospitalization Costs on the use of Test 2. In Figure 13, we consider the impact of the unit quarantine and hospitalization costs on the use of the cheaper Test 2, as opposed to the more expensive Test 1. As we see in the figure, during the early and late phases of the epidemic, larger unit quarantine and hospitalization costs favor the use of more expensive and accurate Test 1. The interesting observation, on the other hand, is that during the active phase of the epidemic, on the other hand, the quarantine and hospitalization unit costs has no discernible impact on the choice of accurate and expensive Test 1 versus less-accurate and cheaper Test 2.

4.3 Multi-City Epidemic Dynamics

We next use SIRTEM to investigate the multi-city dynamics, with intra- and inter-city mixing. In particular, we consider 11 cities/regions[1] in Maricopa county, Arizona, under home, work, and other mixing as described in Section 3.1.2. Figure 14 provides an overview of the average mixing rates for all phases of the epidemic reported in Table 6 against the size of the population. As expected, the mixing rate is generally inversely correlated with the population size of the city – the larger the city, the less likelihood for any pair of individuals to meet (note that the chart does not explicitly show the cross-city mixing rates).

Once again, we consider a scenario where there are two diagnostic tests and a serology test. The high accuracy test has sensitivity 0.75 and specificity 0.95. The low accuracy test has sensitivity 0.65 and specificity 0.85. For both tests, we consider the testing rate, ϕ, to be 0.01 for asymptomatic population and 0.2 for symptomatic population. The model also includes an accurate serology test with the test rate, ϕ, value of 0.01.

In Figures 15 and 16, we investigate the impact of various key parameters on the multi-city epidemic dynamics. In particular, we consider two distinct per-contact transmission rates 0.05 and 0.1 for COVID-19 (roughly covering the range of values reported in the literature) and consider initial infected population sizes of $\sim$ 80 (the reported cases

[1]We selected the 10 largest cities in Maricopa county, Arizona, with respect to the population size and worker movement and merged the remaining small cities under a single region label, "Others". For mixing rate computations, the distance of this aggregate region to a given city has been approximated as half of the maximum distance of the city to all the cities in the aggregate region.

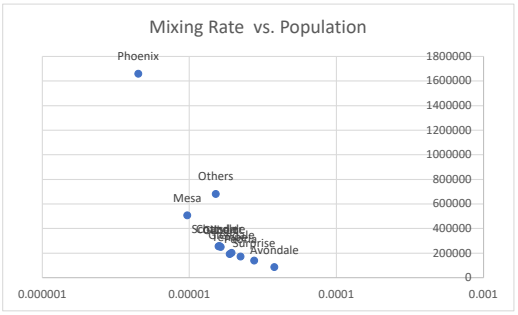

Fig. 14. Per-city mixing rate vs. population for Maricopa County cities: the mixing rate is generally inversely correlated with the population size of the city (the larger the city, the less likelihood for any pair of individuals to meet) (X-axis: mixing rate; Y-Axis: Population)

on 03/22/2020) [75] and $\sim$ 400, assuming that the number of real cases in the population is 5$\times$ those of the reported infections. The Y-axis in the charts denote the level of exposed individuals before the per-day exposure rate crests in the population; i.e., when the epidemic starts to decline. We denote this as the *exposure at epidemic decline or* EED. Note that, in the SIRTEM model, exposed individuals develop symptomatic or asymptomatic COVID-19 – therefore, this is also the level of the infected individuals in the population before the eopidemic starts to decline.

As we see in Figure 15, the EED rate is generally between 35% and 65%, with the population size being highly correlated with EED. We see in the charts that, in general, the larger the population, the higher the EED; the correlation, however, is not perfect due to variations in work-related inter-city mixing. In these charts, we also see that, as expected, a lower per-contact transmission rate (Figure 15(b)) results in a lower EED, especially for smaller cities. As expected, an overall higher mixing rate also results in a larger EED (Figure 15(c)). Interestingly, on the other hand, a higher initial population does not necessarily result in a larger EED (Figure 15(d)) – while the disease grows faster in the population, the EED is not significantly impacted by the size of the initial infected population.

Finally, Figure 16 shows the average impact of work-related movement (as a ratio of the cities' own populations) to the EED rate. As we see here, some cities (such as Tempe) have relatively large work-related movement considering their own populations, whereas others (such as Mesa) have a much lower work-related movement as a ratio of the population. As we see in the figure, even during the lockdowns, the work-related movements within and across cities has a slight, but generally positive impact on the EED of the epidemic.

5 CONCLUSIONS

Epidemic testing strategies are designed with three complementary objectives: (a) Obtaining a faithful picture of the COVID-19 model as well as epidemic trajectory; (b) identifying individuals and populations who are at risk of exposure or are already sick; and (c) guiding intervention efforts, such as isolation of infectious individuals, quarantining of suspected contacts, and minimization go contact rates without completely disrupting the society. To achieve these goals, the testing strategy should account for several practical constraints, such as the daily testing capacity, limitations for different testing types and the potential of the epidemic to disrupt the healthcare infrastructure if we fail in identifying dangerous outbreaks. For this, we need to account for the spatial distribution and mobility of the susceptible population as well as the sensitivity and specificity of the available tests. In particular, testing can be a costly process especially during the onset of an epidemic and accuracy of available tests can have significant impact on the epidemic progress: When test sensitivity accuracy is low, we will not be able to separate the infected population efficiently from the healthy

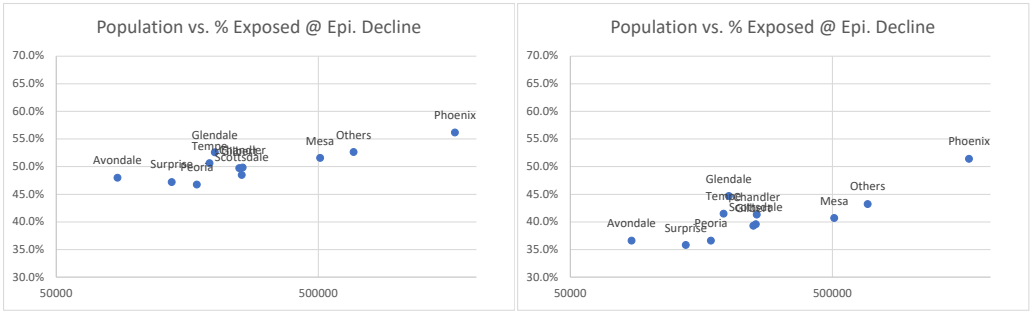

(a) $t = 0.1$, $i = 82$

(b) $t = 0.05$, $i = 82$

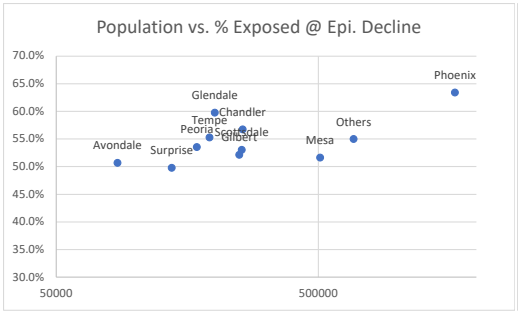

(c) $t = 0.1$, $i = 82$, high mixing

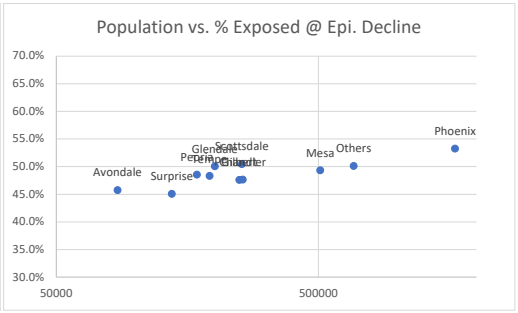

(d) $t = 0.1$, $i = 430$

Fig. 15. Population vs. the level (EED) of exposed individuals before the per-day exposure rate crests in the population. In these charts, t denotes the per-contact transmission rate of the disease and i denotes the size of the initial population who are sick in the Maricopa county; the default mixing rates are the lock-down mixing rates described in Table 6 in Section 3.1.2, whereas "high mix" corresponds to a scenario with weaker lockdown where the entire simulation is ran under $work = 1.25$, $home = 2$, and $other = 2$ (X-axis: mixing rate; Y-Axis: percent exposure)

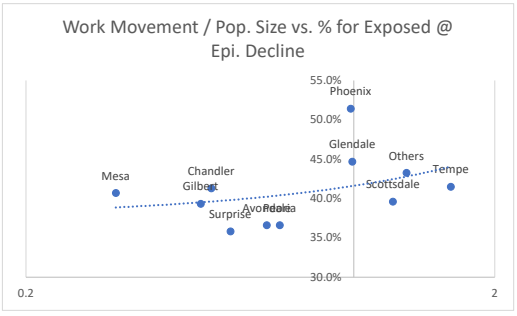

Fig. 16. Work related movement vs. the level (EED) of exposed individuals before the per-day exposure rate crests in the population; in this chart, per-contact transmission rate is 0.05 whereas the initial infected population is 82 (X-axis: work movement/population; Y-Axis: percent exposure)

population, resulting in a spike in disease spread. On the other hand, if the specificity accuracy is low, we can falsely quarantine healthy individuals. In this paper, we presented a novel spatially-informed epidemic model, SIRTEM (for

"*Spatially Informed Rapid Testing for Epidemic Modeling*") that integrates multi-accuracy testing strategies, along with quarantine and hospitalization processes. The model is coupled with an optimization model that incorporates spatially based testing and hospitalization resource constraints. We presented extensive experiments that shows the utility of SIRTEM and the associated optimization model in both single-city and multi-city scenarios.

6 APPENDICES

Case	Cap.T1	Cap.T2	Max H.Bed	Sen.T1	Sen.T2	Spe. T1	Spe.T2	Co.T1	Co.T2	Q.Cost	H.Cost
Case 1	24,349	26,000	1,024	0.75	0.71	0.95	0.81	50	18	30	1,603
Case 2	12,050	26,894	1,143	0.75	0.67	0.95	0.82	50	7	163	4,268
Case 3	21,986	63,310	1,235	0.75	0.65	0.95	0.76	50	8	141	3,818
Case 4	20,431	47,689	1,657	0.75	0.75	0.95	0.72	50	50	199	4,975
Case 5	16,127	36,959	1,398	0.75	0.63	0.95	0.86	50	47	4	1,071
Case 6	17,978	25,328	1,256	0.75	0.61	0.95	0.71	50	47	16	1,321
Case 7	22,551	46,142	1,474	0.75	0.66	0.95	0.74	50	1	171	4,414
Case 8	12,889	24,399	1,699	0.75	0.71	0.95	0.73	50	23	104	3,081
Case 9	24,519	53,270	1,705	0.75	0.55	0.95	0.92	50	29	79	2,585
Case 10	20,811	40,944	1,815	0.75	0.53	0.95	0.87	50	40	127	3,536
Case 11	19,303	48,640	1,934	0.75	0.74	0.95	0.73	50	16	48	1,962
Case 12	16,879	37,890	1,854	0.75	0.72	0.95	0.75	50	35	64	2,289
Case 13	20,730	43,578	1,449	0.75	0.69	0.95	0.86	50	18	13	1,267
Case 14	15,017	24,136	1,210	0.75	0.58	0.95	0.79	50	32	193	4,868
Case 15	22,957	48,826	1,485	0.75	0.52	0.95	0.71	50	14	151	4,012
Case 16	15,407	16,719	1,861	0.75	0.52	0.95	0.75	50	41	25	1,504
Case 17	15,400	20,159	1,518	0.75	0.70	0.95	0.90	50	22	130	3,598
Case 18	22,158	45,124	1,324	0.75	0.59	0.95	0.77	50	16	115	3,300
Case 19	14,058	38,234	1,559	0.75	0.67	0.95	0.89	50	8	95	2,892
Case 20	11,461	15,159	1,400	0.75	0.70	0.95	0.78	50	33	91	2,826
Case 21	19,790	35,043	1,270	0.75	0.64	0.95	0.85	50	20	101	3,025
Case 22	11,655	15,934	1,997	0.75	0.62	0.95	0.92	50	4	183	4,665
Case 23	18,159	44,931	1,959	0.75	0.72	0.95	0.89	50	25	97	2,930
Case 24	18,495	26,854	1,835	0.75	0.60	0.95	0.80	50	1	7	1,132
Case 25	14,494	16,408	1,779	0.75	0.57	0.95	0.79	50	3	57	2,142
Case 26	20,160	24,698	1,784	0.75	0.50	0.95	0.70	50	30	117	3,332
Case 27	13,409	39,921	1,636	0.75	0.73	0.95	0.91	50	38	165	4,291
Case 28	14,675	43,221	1,172	0.75	0.66	0.95	0.78	50	11	60	2,204
Case 29	19,278	53,500	1,918	0.75	0.60	0.95	0.87	50	43	68	2,370
Case 30	16,940	42,896	1,284	0.75	0.64	0.95	0.76	50	14	22	1,448
Case 31	22,794	28,839	1,973	0.75	0.56	0.95	0.90	50	38	187	4,742
Case 32	10,340	29,210	1,362	0.75	0.55	0.95	0.83	50	10	110	3,202
Case 33	12,300	22,461	1,616	0.75	0.54	0.95	0.82	50	26	158	4,164
Case 34	10,091	26,331	1,669	0.75	0.74	0.95	0.84	50	10	146	3,922
Case 35	18,806	22,485	1,097	0.75	0.63	0.95	0.72	50	24	175	4,505

Table 10. The parameter setting for Single City Model(case 1-35)

Case	Cap.T1	Cap.T2	Max H.Bed	Sen.T1	Sen.T2	Spe.T1	Spe.T2	Co.T1	Co.T2	Q.Cost	H.Cost
Case 36	10,731	16,884	1,056	0.75	0.59	0.95	0.85	50	24	134	3,690
Case 37	15,722	25,842	1,307	0.75	0.58	0.95	0.80	50	27	35	1,691
Case 38	17,323	25,779	1,101	0.75	0.53	0.95	0.88	50	46	82	2,646
Case 39	23,376	60,585	1,585	0.75	0.68	0.95	0.77	50	43	43	1,861
Case 40	21,544	41,739	1,340	0.75	0.73	0.95	0.81	50	32	9	1,190
Case 41	13,037	20,024	1,528	0.75	0.51	0.95	0.88	50	49	48	1,954
Case 42	17,662	32,822	1,008	0.75	0.68	0.95	0.94	50	35	53	2,050
Case 43	21,269	51,610	1,124	0.75	0.57	0.95	0.91	50	5	39	1,778
Case 44	12,522	21,463	1,732	0.75	0.62	0.95	0.95	50	4	190	4,800
Case 45	24,978	59,681	1,064	0.75	0.69	0.95	0.94	50	44	156	4,111
Case 46	23,789	41,232	1,434	0.75	0.56	0.95	0.83	50	20	177	4,547
Case 47	11,112	11,314	1,189	0.75	0.61	0.95	0.74	50	13	138	3,754
Case 48	23,873	69,407	1,742	0.75	0.51	0.95	0.93	50	40	87	2,749
Case 49	16,370	43,315	1,567	0.75	0.54	0.95	0.93	50	30	124	3,474
Case 50	13,873	38,073	1,898	0.75	0.65	0.95	0.84	50	36	74	2,480

Table 11. The parameter setting for Single City Model(case 36-50)

REFERENCES

[1] Jacob B Aguilar and Juan B Gutierrez. 2020. An Epidemiological Model of Malaria Accounting for Asymptomatic Carriers. *Bulletin of Mathematical Biology* 82, 3 (2020), 1–55.

[2] Christian L Althaus. 2014. Estimating the reproduction number of Ebola virus (EBOV) during the 2014 outbreak in West Africa. *PLoS currents* 6 (2014).

[3] Roy M Anderson, B Anderson, and Robert M May. 1992. *Infectious diseases of humans: dynamics and control.* Oxford university press, na.

[4] Roy M Anderson, Hans Heesterbeek, Don Klinkenberg, and T Déirdre Hollingsworth. 2020. How will country-based mitigation measures influence the course of the COVID-19 epidemic? *The Lancet* 395, 10228 (2020), 931–934.

[5] Hakan Andersson and Tom Britton. 2012. *Stochastic epidemic models and their statistical analysis.* Vol. 151. Springer Science & Business Media, na.

[6] Suwardi Annas, Muh Isbar Pratama, Muh Rifandi, Wahidah Sanusi, and Syafruddin Side. 2020. Stability analysis and numerical simulation of SEIR model for pandemic COVID-19 spread in Indonesia. *Chaos, Solitons & Fractals* 139 (2020), 110072.

[7] Jayrold P Arcede, Randy L Caga-Anan, Cheryl Q Mentuda, and Youcef Mammeri. 2020. Accounting for Symptomatic and Asymptomatic in a SEIR-type model of COVID-19. *Mathematical Modelling of Natural Phenomena* 15 (2020), 34.

[8] Mayara Lisboa Bastos, Gamuchirai Tavaziva, Syed Kunal Abidi, Jonathon R Campbell, Louis-Patrick Haraoui, James C Johnston, Zhiyi Lan, Stephanie Law, Emily MacLean, Anete Trajman, et al. 2020. Diagnostic accuracy of serological tests for covid-19: systematic review and meta-analysis. *bmj* 370 (2020), na.

[9] Tom Britton. 2010. Stochastic epidemic models: a survey. *Mathematical biosciences* 225, 1 (2010), 24–35.

[10] Jack H Buckner, Gerardo Chowell, and Michael R Springborn. 2021. Dynamic prioritization of COVID-19 vaccines when social distancing is limited for essential workers. *Proceedings of the National Academy of Sciences* 118, 16 (2021), na.

[11] United States Census Bureau. [n.d.]. *Work Destination Analysis.* https://onthemap.ces.census.gov/

[12] Liming Cai, Xuezhi Li, Mini Ghosh, and Baozhu Guo. 2009. Stability analysis of an HIV/AIDS epidemic model with treatment. *Journal of computational and applied mathematics* 229, 1 (2009), 313–323.

[13] José M Carcione, Juan E Santos, Claudio Bagaini, and Jing Ba. 2020. A simulation of a COVID-19 epidemic based on a deterministic SEIR model. *Frontiers in public health* 8 (2020), 230.

[14] CDC. [n.d.]. *When to Quarantine.* https://www.cdc.gov/coronavirus/2019-ncov/hcp/planning-scenarios.html

[15] Derek K Chu, Elie A Akl, Stephanie Duda, Karla Solo, Sally Yaacoub, Holger J Schünemann, Amena El-harakeh, Antonio Bognanni, Tamara Lotfi, Mark Loeb, et al. 2020. Physical distancing, face masks, and eye protection to prevent person-to-person transmission of SARS-CoV-2 and COVID-19: a systematic review and meta-analysis. *The Lancet* (2020).

[16] Dmytro Chumachenko, Ievgen Meniailov, Kseniia Bazilevych, Yuliia Kuznetsova, and Tetyana Chumachenko. 2019. Development of an intelligent agent-based model of the epidemic process of syphilis. In *2019 IEEE 14th International Conference on Computer Sciences and Information Technologies (CSIT)*, Vol. 1. IEEE, 42–45.

[17] CTW. [n.d.]. *The Covid Tracking Project.* https://covidtracking.com/data

[18] Erik Cuevas. 2020. An agent-based model to evaluate the COVID-19 transmission risks in facilities. *Computers in biology and medicine* 121 (2020), 103827.

[19] Emma L Davis, Tim CD Lucas, Anna Borlase, Timothy M Pollington, Sam Abbott, Diepreye Ayabina, Thomas Crellen, Joel Hellewell, Li Pi, Graham F Medley, et al. 2020. An imperfect tool: COVID-19'test & trace'success relies on minimising the impact of false negatives and continuation of physical distancing. *medRxiv* (2020).

[20] Wei Duan, Zongchen Fan, Peng Zhang, Gang Guo, and Xiaogang Qiu. 2015. Mathematical and computational approaches to epidemic modeling: a comprehensive review. *Frontiers of Computer Science* 9, 5 (2015), 806–826.

[21] Chris Dye and Nigel Gay. 2003. Modeling the SARS epidemic. *Science* 300, 5627 (2003), 1884–1885.

[22] Steffen E Eikenberry, Marina Mancuso, Enahoro Iboi, Tin Phan, Keenan Eikenberry, Yang Kuang, Eric Kostelich, and Abba B Gumel. 2020. To mask or not to mask: Modeling the potential for face mask use by the general public to curtail the COVID-19 pandemic. *Infectious Disease Modelling* 5 (2020), 293–308.

[23] Ralf Engbert, Maximilian M Rabe, Reinhold Kliegl, and Sebastian Reich. 2021. Sequential data assimilation of the stochastic SEIR epidemic model for regional COVID-19 dynamics. *Bulletin of mathematical biology* 83, 1 (2021), 1–16.

[24] Ru Guo Fan, Yi Bo Wang, Ming Luo, Ying Qing Zhang, and Chao Ping Zhu. 2020. SEIR-Based COVID-19 Transmission Model and Inflection Point Prediction Analysis. *Dianzi Keji Daxue Xuebao/Journal of the University of Electronic Science and Technology of China* 49, 3 (2020).

[25] Dennis M Feehan and Ayesha S Mahmud. 2021. Quantifying population contact patterns in the United States during the COVID-19 pandemic. *Nature communications* 12, 1 (2021), 1–9.

[26] Enrique Frias-Martinez, Graham Williamson, and Vanessa Frias-Martinez. 2011. An agent-based model of epidemic spread using human mobility and social network information. In *2011 IEEE third international conference on privacy, security, risk and trust and 2011 IEEE third international conference on social computing*. IEEE, 57–64.

[27] Jacob R Gardner, Matt J Kusner, Zhixiang Eddie Xu, Kilian Q Weinberger, and John P Cunningham. 2014. Bayesian Optimization with Inequality Constraints.. In *ICML*, Vol. 2014. 937–945.

[28] Salah Ghamizi, Renaud Rwemalika, Maxime Cordy, Lisa Veiber, Tegawendé F Bissyandé, Mike Papadakis, Jacques Klein, and Yves Le Traon. 2020. Data-driven simulation and optimization for covid-19 exit strategies. In *Proceedings of the 26th ACM SIGKDD International Conference on Knowledge Discovery & Data Mining*. 3434–3442.

[29] Chaitra Gopalappa, Paul G Farnham, Yao-Hsuan Chen, and Stephanie L Sansom. 2017. Progression and transmission of HIV/AIDS (PATH 2.0) a new, agent-based model to estimate HIV transmissions in the United States. *Medical Decision Making* 37, 2 (2017), 224–233.

[30] Michael Greenstone and Vishan Nigam. 2020. Does social distancing matter? *University of Chicago, Becker Friedman Institute for Economics Working Paper* 2020-26 (2020).

[31] Jürgen Hackl and Thibaut Dubernet. 2019. Epidemic spreading in urban areas using agent-based transportation models. *Future internet* 11, 4 (2019), 92.

[32] F Binti Hamzah, C Lau, H Nazri, DV Ligot, G Lee, CL Tan, MKM Shaib, UH Zaidon, A Abdullah, MH Chung, et al. 2020. CoronaTracker: worldwide COVID-19 outbreak data analysis and prediction. *Bull World Health Organ* 1, 32 (2020), na.

[33] Shaobo He, Yuexi Peng, and Kehui Sun. 2020. SEIR modeling of the COVID-19 and its dynamics. *Nonlinear Dynamics* (2020), 1–14.

[34] Nicolas Hoertel, Martin Blachier, Carlos Blanco, Mark Olfson, Marc Massetti, Frederic Limosin, and Henri Leleu. 2020. Facing the COVID-19 epidemic in NYC: a stochastic agent-based model of various intervention strategies. *MedRxiv* (2020).

[35] Ismail Husein, Dwi Noerjoedianto, Muhammad Sakti, and Abeer Hamoodi Jabbar. 2020. Modeling of Epidemic Transmission and Predicting the Spread of Infectious Disease. *Systematic Reviews in Pharmacy* 11, 6 (2020).

[36] Mark Jit and Marc Brisson. 2011. Modelling the epidemiology of infectious diseases for decision analysis. *Pharmacoeconomics* 29, 5 (2011), 371–386.

[37] De Kai, Guy-Philippe Goldstein, Alexey Morgunov, Vishal Nangalia, and Anna Rotkirch. 2020. Universal masking is urgent in the covid-19 pandemic: Seir and agent based models, empirical validation, policy recommendations. *arXiv preprint arXiv:2004.13553* (2020).

[38] Cliff C Kerr, Robyn M Stuart, Dina Mistry, Romesh G Abeysuriya, Gregory Hart, Katherine Rosenfeld, Prashanth Selvaraj, Rafael C Nunez, Brittany Hagedorn, Lauren George, et al. 2020. Covasim: an agent-based model of COVID-19 dynamics and interventions. *medRxiv* (2020).

[39] Soyoung Kim, Yae-Jean Kim, Kyong Ran Peck, and Eunok Jung. 2020. School opening delay effect on transmission dynamics of coronavirus disease 2019 in Korea: based on mathematical modeling and simulation study. *Journal of Korean medical science* 35, 13 (2020).

[40] Moritz UG Kraemer, Chia-Hung Yang, Bernardo Gutierrez, Chieh-Hsi Wu, Brennan Klein, David M Pigott, Louis Du Plessis, Nuno R Faria, Ruoran Li, William P Hanage, et al. 2020. The effect of human mobility and control measures on the COVID-19 epidemic in China. *Science* 368, 6490 (2020), 493–497.

[41] Toshikazu Kuniya and Hisashi Inaba. 2020. Possible effects of mixed prevention strategy for COVID-19 epidemic: massive testing, quarantine and social distancing. *AIMS public health* 7, 3 (2020), 490.

[42] Phenyo E Lekone and Bärbel F Finkenstädt. 2006. Statistical inference in a stochastic epidemic SEIR model with control intervention: Ebola as a case study. *Biometrics* 62, 4 (2006), 1170–1177.

[43] Michael Y Li and James S Muldowney. 1995. Global stability for the SEIR model in epidemiology. *Mathematical biosciences* 125, 2 (1995), 155–164.
[44] Ruiyun Li, Sen Pei, Bin Chen, Yimeng Song, Tao Zhang, Wan Yang, and Jeffrey Shaman. 2020. Substantial undocumented infection facilitates the rapid dissemination of novel coronavirus (SARS-CoV-2). *Science* 368, 6490 (2020), 489–493.
[45] Qun Liu, Daqing Jiang, Tasawar Hayat, and Ahmed Alsaedi. 2019. Dynamical behavior of a stochastic epidemic model for cholera. *Journal of the Franklin Institute* 356, 13 (2019), 7486–7514.
[46] Leonardo López and Xavier Rodo. 2021. A modified SEIR model to predict the COVID-19 outbreak in Spain and Italy: simulating control scenarios and multi-scale epidemics. *Results in Physics* 21 (2021), 103746.
[47] Dejen Ketema Mamo and Purnachandra Rao Koya. 2015. Mathematical modeling and simulation study of SEIR disease and data fitting of Ebola epidemic spreading in West Africa. *Journal of Multidisciplinary Engineering Science and Technology* 2, 1 (2015), 106–114.
[48] Google Maps. [n.d.]. *Distances between cities.* https://www.google.com/maps
[49] Florian Miksch, Philipp Pichler, Kurt JP Espinosa, Katrina ST Casera, Aldrin N Navarro, and Martin Bicher. 2015. An agent-based epidemic model for dengue simulation in the Philippines. In *2015 Winter Simulation Conference (WSC)*. IEEE, 3202–3203.
[50] George J Milne and Simon Xie. 2020. The effectiveness of social distancing in mitigating COVID-19 spread: a modelling analysis. *medRxiv* (2020).
[51] Samuel Mwalili, Mark Kimathi, Viona Ojiambo, Duncan Gathungu, and Rachel Mbogo. 2020. SEIR model for COVID-19 dynamics incorporating the environment and social distancing. *BMC Research Notes* 13, 1 (2020), 1–5.
[52] Ram Naresh, Agraj Tripathi, and Sandip Omar. 2006. Modelling the spread of AIDS epidemic with vertical transmission. *Appl. Math. Comput.* 178, 2 (2006), 262–272.
[53] Calistus N Ngonghala, Enahoro Iboi, Steffen Eikenberry, Matthew Scotch, Chandini Raina MacIntyre, Matthew H Bonds, and Abba B Gumel. 2020. Mathematical assessment of the impact of non-pharmaceutical interventions on curtailing the 2019 novel Coronavirus. *Mathematical biosciences* 325 (2020), 108364.
[54] NPR. 2020. CDC Report: Officials Knew Coronavirus Test Was Flawed But Released It Anyway. https://www.npr.org/2020/11/06/929078678/cdc-report-officials-knew-coronavirus-test-was-flawed-but-released-it-anyway?t=1622449349652
[55] Ryosuke Omori, Kenji Mizumoto, and Gerardo Chowell. 2020. Changes in testing rates could mask the novel coronavirus disease (COVID-19) growth rate. *International Journal of Infectious Diseases* 94 (2020), 116–118.
[56] A David Paltiel, Amy Zheng, and Rochelle P Walensky. 2020. Assessment of SARS-CoV-2 screening strategies to permit the safe reopening of college campuses in the United States. *JAMA network open* 3, 7 (2020), e2016818–e2016818.
[57] Gaurav Pandey, Poonam Chaudhary, Rajan Gupta, and Saibal Pal. 2020. SEIR and Regression Model based COVID-19 outbreak predictions in India. *arXiv preprint arXiv:2004.00958* (2020).
[58] Jasmina Panovska-Griffiths, Cliff C Kerr, Robyn M Stuart, Dina Mistry, Daniel J Klein, Russell M Viner, and Chris Bonell. 2020. Determining the optimal strategy for reopening schools, the impact of test and trace interventions, and the risk of occurrence of a second COVID-19 epidemic wave in the UK: a modelling study. *The Lancet Child & Adolescent Health* 4, 11 (2020), 817–827.
[59] Sang Woo Park, Kaiyuan Sun, Cécile Viboud, Bryan T Grenfell, and Jonathan Dushoff. 2020. Potential role of social distancing in mitigating spread of coronavirus disease, South Korea. *Emerging infectious diseases* 26, 11 (2020), 2697.
[60] Facundo Piguillem and Liyan Shi. 2020. Optimal COVID-19 quarantine and testing policies. (2020).
[61] The Covid Tracking Project. [n.d.]. *Covid-19 Positive Negative cases.* https://covidtracking.com/
[62] Amirarsalan Rajabi, Alexander V Mantzaris, Ece C Mutlu, and Ivan Garibay. 2020. Investigating dynamics of covid-19 spread and containment with agent-based modeling. *medRxiv* (2020).
[63] Timothy C Reluga. 2010. Game theory of social distancing in response to an epidemic. *PLoS Comput Biol* 6, 5 (2010), e1000793.
[64] Alisa Joy Rhee. 2006. *An agent-based approach to HIV/AIDS epidemic modeling: a case study of Papua New Guinea.* Ph.D. Dissertation. Massachusetts Institute of Technology.
[65] Rebecca J Rockett, Alicia Arnott, Connie Lam, Rosemarie Sadsad, Verlaine Timms, Karen-Ann Gray, John-Sebastian Eden, Sheryl Chang, Mailie Gall, Jenny Draper, et al. 2020. Revealing COVID-19 transmission in Australia by SARS-CoV-2 genome sequencing and agent-based modeling. *Nature medicine* 26, 9 (2020), 1398–1404.
[66] Marc Saez, Aurelio Tobias, Diego Varga, and Maria Antònia Barceló. 2020. Effectiveness of the measures to flatten the epidemic curve of COVID-19. The case of Spain. *Science of the Total Environment* (2020), 138761.
[67] Eunha Shim, Amna Tariq, Wongyeong Choi, Yiseul Lee, and Gerardo Chowell. 2020. Transmission potential and severity of COVID-19 in South Korea. *International Journal of Infectious Diseases* 93 (2020), 339–344.
[68] Constantinos Siettos, Cleo Anastassopoulou, Lucia Russo, Christos Grigoras, and Eleftherios Mylonakis. 2015. Modeling the 2014 ebola virus epidemic–agent-based simulations, temporal analysis and future predictions for liberia and sierra leone. *PLoS currents* 7 (2015).
[69] Petrônio CL Silva, Paulo VC Batista, Hélder S Lima, Marcos A Alves, Frederico G Guimarães, and Rodrigo CP Silva. 2020. COVID-ABS: An agent-based model of COVID-19 epidemic to simulate health and economic effects of social distancing interventions. *Chaos, Solitons & Fractals* 139 (2020), 110088.
[70] Statista. [n.d.]. *covid-19-impact-on-the-global-economy.* https://www.statista.com/topics/6139/covid-19-impact-on-the-global-economy/
[71] Angela Felicia Sunjaya and Anthony Paulo Sunjaya. 2020. Pooled testing for expanding COVID-19 mass surveillance. *Disaster Medicine and Public Health Preparedness* 14, 3 (2020), e42–e43.

[72] Elena Surkova, Vladyslav Nikolayevskyy, and Francis Drobniewski. 2020. False-positive COVID-19 results: hidden problems and costs. *The Lancet Respiratory Medicine* 8, 12 (2020), 1167–1168.

[73] Jouni T Tuomisto, Juha Yrjölä, Mikko Kolehmainen, Juhani Bonsdorff, Jami Pekkanen, and Tero Tikkanen. 2020. An agent-based epidemic model REINA for COVID-19 to identify destructive policies. *medRxiv* (2020).

[74] Buddhisha Udugama, Pranav Kadhiresan, Hannah N Kozlowski, Ayden Malekjahani, Matthew Osborne, Vanessa YC Li, Hongmin Chen, Samira Mubareka, Jonathan B Gubbay, and Warren CW Chan. 2020. Diagnosing COVID-19: the disease and tools for detection. *ACS nano* 14, 4 (2020), 3822–3835.

[75] John Hopkins University. [n.d.]. *John Hopkins University Corona Virus Resource Center.* https://coronavirus.jhu.edu/us-map

[76] Rochelle P Walensky and Carlos Del Rio. 2020. From mitigation to containment of the COVID-19 pandemic: putting the SARS-CoV-2 genie back in the bottle. *Jama* na, na (2020), na.

[77] Chad R Wells, Jeffrey P Townsend, Abhishek Pandey, Seyed M Moghadas, Gary Krieger, Burton H Singer, Robert H McDonald, Meagan C Fitzpatrick, and Alison P Galvani. 2020. Optimal COVID-19 quarantine and testing strategies. *medRxiv* (2020).

[78] WHO. [n.d.]. *World Health Organization Covid-19 Dashbpard.* https://covid19.who.int/

[79] Christopher Wolfram. 2020. An agent-based model of covid-19. *Complex Systems* 29, 1 (2020).

[80] Conghui Xu, Yongguang Yu, QuanChen Yang, and Zhenzhen Lu. 2020. Forecast analysis of the epidemics trend of COVID-19 in the United States by a generalized fractional-order SEIR model. *arXiv preprint arXiv:2004.12541* (2020).

[81] Zifeng Yang, Zhiqi Zeng, Ke Wang, Sook-San Wong, Wenhua Liang, Mark Zanin, Peng Liu, Xudong Cao, Zhongqiang Gao, Zhitong Mai, et al. 2020. Modified SEIR and AI prediction of the epidemics trend of COVID-19 in China under public health interventions. *Journal of thoracic disease* 12, 3 (2020), 165.

[82] Hongjun Zhao, Xiaoxiao Lu, Yibin Deng, Yujin Tang, and Jiachun Lu. 2020. COVID-19: asymptomatic carrier transmission is an underestimated problem. *Epidemiology & Infection* 148 (2020).